FRICTION STIR PROCESSING OF POWDER METALLURGICAL Al ALLOYS

A DISSERTATION

Submitted in partial fulfillment of the
requirements for the award of the degree
of
MASTER OF TECHNOLOGY
in
METALLURGICAL AND MATERIALS ENGINEERING
(With Specialization in Industrial Metallurgy)

By

SUPRATIM ENDOW

DEPARTMENT OF METALLURGICAL AND MATERIALS ENGINEERING
INDIAN INSTITUTE OF TECHNOLOGY ROORKEE
ROORKEE – 247 667 (INDIA)
MAY, 2016

CANDIDATE'S DECLARATION

I hereby declare that the proposed work presented in this dissertation entitled **"Friction Stir Processing of Powder Metallurgical Al Alloys"** in partial fulfilment of the requirements for the award of the degree of **Master of Technology** in **Metallurgical and Materials Engineering** with specialization in Industrial Metallurgy, submitted in the **Department of Metallurgical and Materials Engineering, Indian Institute of Technology Roorkee** is an authentic record of my own work carried out during the period from July 2015 to May 2016 under the supervision of **Dr. V. Pancholi**, Associate Professor, Department of Metallurgical and Materials Engineering, Indian Institute of Technology Roorkee and **Dr. V. V. Dabhade**, Associate Professor, Department of Metallurgical and Materials Engineering, Indian Institute of Technology Roorkee. The matter presented in this dissertation has not been submitted by me for the award of any other degree.

Dated:

Place: Roorkee **SUPRATIM ENDOW**

CERTIFICATE

This is to certify that the above statement made by the candidate is correct to the best of my knowledge and belief.

Dr. V. Pancholi,
Associate Professor,
Department of Metallurgical
and Materials Engineering,
Indian Institute of Technology Roorkee.

Dr. V. V. Dabhade,
Associate Professor
Department of Metallurgical
and Materials Engineering
Indian Institute of Technology,Roorkee

ACKNOWLEDGEMENTS

The project on "Friction Stir Processing of Powder Metallurgical Al Alloys" has been a journey that was both exciting and educational. Apart from my own effort, the completion of my project depends enormously on the motivational effort of a few other people. I take this opportunity in expressing my heartfelt gratitude and sincere thanks to all those people who have been involved in the successful completion of my project.

Above all, I would like to show my deep sense of gratitude to my supervisors, Dr. V. Pancholi, Associate Professor, Department of Metallurgical and Materials Engineering, Indian Institute of Technology Roorkee and Dr. V. V. Dabhade, Assistant Professor, Department of Metallurgical and Materials Engineering, Indian Institute of Technology Roorkee for their guidance and advice throughout the project work. The project was born through their encouragement and lived through their guidelines and supervision.

Sincere thanks to Mr. Aniruddha Malakar, Mr. A. Raja, Mr. Suresh Sonkar, Mr. Rahul Kumar, Mr. Kuldeep Saxena, Mr. R Sunil Kumar and Mr. Tilak Joshi for their guidance during the project. I am also thankful to Mr. Rajendra Sharma, Mr. Ashish Kush, Mr. Dinesh Kumar, Mr. Sukhmal Giri, Mr. Naresh Sharma and Mr. Dhan Prakash for their help during the experimental work.

I would also like to convey my heartfelt thanks to Dr. Anjan Sil, Professor and Head, Department of Metallurgical and Materials Engineering, Indian Institute of Technology Roorkee for providing me all necessary facilities in the department to complete this work.

Last but not the least, my sincere thanks to my parents who have been a constant source of my inspiration to me and I am also grateful to my friends who have provided suggestions at different stages of my work.

Supratim Endow

ABSTRACT

Friction stir processing (FSP) is used for microstructural modifications in powder metallurgical aluminium alloys. It serves the purpose of grain refinement, reduction in porosity, homogenisation and thus improves the mechanical properties of the alloy. In this case, study has been carried out to determine (i) effect of compaction pressure on FSP of pure aluminium compact, (ii) difference between the properties of green and sintered compacts of pure aluminium after FSP and (iii) the effect of addition of copper into aluminium matrix. The green compacts were synthesized using Cold Isostatic Press (CIP) machine at seven different compaction pressures which were 50 MPa, 100 MPa, 150 MPa, 200 MPa, 250 MPa, 320 MPa and 380 MPa. FSP was carried out on all the green compacts using process parameters of 1525 rpm and 1mm/min. It was found that FSP was possible on all the green compacts. After FSP, the value of density reached almost equivalent to that of theoretical density. Moreover, intense plastic deformation and high heat generation during FSP causes dynamic recrystallization which results in the generation of fine grains. As a result the mechanical properties after FSP were highly enhanced. It was observed that if the sample was prepared using either too high or too low compaction pressure then during FSP the material movement was hindered. In this study, 200 MPa compaction pressure was found to be optimum for proper material movement during FSP as it has shown ultimate tensile strength (UTS) of 153 MPa and ductility of 38% which is highest among all the samples. Sintering was carried out on this sample in an atmosphere of N_2 gas and subjected to FSP to find out the difference between the effect of FSP on green and sintered samples. The mechanical properties of the sintered sample was then compared with the green compact. Electron Back Scattered Diffraction (EBSD) was done to find out the reduction in grain size after FSP. Fractography revealed that after FSP, the fracture surface showed predominant dimple morphology to aid to its ductile property. Copper was also added to pure aluminium in three different compositions of Al-1wt%Cu, Al-5wt%Cu and Al-10wt%Cu and its effect on the properties was studied. It was found that the UTS of Al-1wt%Cu and Al-5wt%Cu was more in comparision to pure aluminium but it decreased in case of Al-10%Cu with significant reduction in ductility. The reason for such behaviour is attributed to the formation of intermetallics in excess which acted as crack initiation sites and hence resulted in quick failure.

Keywords: Friction Stir Processing, Powder Metallurgy, Aluminium Alloys

TABLE OF CONTENTS

CANDIDATE'S DECLARATION i

ACKNOWLEDGEMENTS ii

ABSTRACT iii

TABLE OF CONTENTS iv

LIST OF FIGURES vii

LIST OF TABLES x

CHAPTER 1 INTRODUCTION **1**

1.1 Powder Metallurgy 1

1.2 Friction Stir Processing 2

1.2.1 *Introduction to Friction Stir Processing* 2

1.2.2 *Working Principle of Friction Stir Processing* 2

1.2.3 *Process Parameters* 2

1.3 Metal Matrix Composites 4

CHAPTER 2 LITERATURE REVIEW **7**

2.1 Macrostructural and microstructural evolution during FSP 7

2.2 Recrystallization Mechanisms 9

2.3 Effect of process parameters on grain size 10

2.4 Applications of friction stir processing on metal matrix composites fabricated through powder metallurgy route 12

2.5 Strengthening mechanisms in Friction Stir Processed composites 15

2.6 Gap in work and objective of my work 17

CHAPTER 3 PLAN OF WORK **18**

CHAPTER 4 EXPERIMENTAL PROCEDURE **21**

4.1 Raw Materials Used 21

4.2 Cold Isostatic Compaction 21
4.2.1 *Pure Aluminium Sample* 21
4.2.2 *Al-Cu Sample* 21
4.3 Friction Stir Processing 22
4.3.1 *Selection of most suitable compaction pressure* 23
4.3.2 *FSP on Al-Cu composites for 3 different compositions* 24
4.4 Porosity Calculation 24
4.5 Microstructure Characterization 24
4.6 Mechanical Testing 26
4.7 XRD Analysis 27
CHAPTER 5 RESULTS AND DISCUSSION 28
5.1 Powder Characterization 28
5.2 Effect of Compaction Pressure on FSPed Pure Aluminium Compact 28
5.2.1 *Microstructure Characterisation* 28
5.2.2 *Density and Porosity* 30
5.2.3 *Mechanical Properties* 32
5.2.3.1 *Hardness* 33
5.2.3.2 *Tensile Properties* 34
5.2.4 *Fractrography* 36
5.3 Comparision between Green FSPed and Sintered FSPed samples compacted at 200 MPa 37
5.3.1 *Microstructure Characterization* 38
5.3.2 *Density and Porosity* 39
5.3.3 *Mechanical Properties* 41
5.3.3.1 *Hardness* 41
5.3.3.2 Tensile Properties 42
5.3.4 *Fractography* 44

5.4 Effect of addition of copper to aluminum matrix 45

5.4.1 *Microstructure Characterization* 45

5.4.2 *Density and Porosity* 47

5.4.3 *XRD Analysis* 49

5.4.4 *Mechanical Properties* 52

5.4.4.1 *Hardness* 52

5.4.4.2 *Tensile Properties* 53

5.4.5 *Fractrography* 55

CHAPTER 6 CONCLUSION 57

CHAPTER 7 SCOPE FOR FUTURE WORK 59

REFERENCES 60

LIST OF PUBLICATIONS 63

LIST OF FIGURES

Fig. 1.1. (a) Schematic of FSP Process and (b) Different pin designs of a FSP tool 3
Fig. 2.1. Metallurgical processing zones developed during FSP..... 7
Fig. 2.2. A typical macrograph highlighting different the different microstructural zones in FSP 7075Al..... 8
Fig. 2.3. Variation in shape of stir zone with processing parameter in FSP A356 (a) basin shaped, 300 rpm/51 mm/min (b) elliptical, 700 rpm/102 mm/min(c) onion shaped, 900 rpm/203 mm/min 9
Fig. 2.4. Effect of FSP process parameters on grain size of nugget zone in FSPed 7075Al at (a) 350 rpm, 152 mm/min and (b) 400 rpm, 102 mm/min..... 10
Fig. 2.5. Distribution of grain size in various sections of 7075Al weld nugget. 11
Fig. 2.6. SEM Image of (a) Al- 15 %Cu sintered at 803 K (b) Al- 15 %Cu sintered at 803 K followed by 2 FSP passes. 13
Fig. 2.7. (a) Fine $Al_{13}Fe_4$ and (b) Fine Al_3Ti particles uniformly distributed in aluminium matrix..... 14
Fig. 2.8. TEM/BFI Image showing the formation of (a) Al_2O_3 particle at the Al/SiO_2 interface and (b) CuO/Cu_2O (C), enclosed by a shell comprised of aluminium oxide (B) and Al_2Cu (A) in FSPed Al–10CuO specimen. 14
Fig. 2.9. XRD patterns of FSPed Al- CeO_2 composite processed using different tool traversing speeds. The FSP was performed (sintered at 883K) with a tool rotating rate of 500 rpm and traverse speed of (a) 30 mm/min (b) 85 mm/min or (c) 120 mm/min. (d) Specimen was sintered at 813 K followed by four FSP passes with parameters, 500 rpm and 30 mm/min 15
Fig.3.1. Flow diagram showing the work plan for determining the optimum compaction pressure 18
Fig.3.2. Flow diagram showing the work plan for comparision between green FSPed and sintered FSPed samples compacted at 200 MPa..... 19
Fig. 3.3. Flow diagram showing the plan of work for determining the effect of copper addition into aluminium matrix 20
Fig. 4.1. Cold Isostatic Press (CIP) Machine..... 22
Fig. 4.2. (a) Friction Stir Processing Machine and (b) FSP tool 22
Fig. 4.3. (a) Tool holder and fixture used during processing (b) A FSPed sample using process parameters as 1525rpm and 1 mm/min..... 23

Fig. 4.4. (a) Buehler Simplimet 1000 automatic press and (b) A hot mounted sample 25
Fig. 4.5. Optical microscope (LEICA,5000M) 25
Fig. 4.6. Scanning electron microscope (ZEISS) 26
Fig. 4.7. Universal testing machine (TINIUS OLSEN,H25KS) 26
Fig. 4.8. Vickers Hardness Tester VM50 PC 27
Fig. 4.9. X-Ray Diffraction (XRD) Machine (Rigaku) 27
Fig. 5.1. SEM Images of (a) pure Al powder and (b) pure Cu powder 28
Fig. 5.2. Electropolished sample compacted at 200 MPa 29
Fig. 5.3. (a) Microstructure of pure Al green compact (b) Microstructure after FSP and (c) Microstructure showing the different regions after FSP 29
Fig. 5.4.(a) EBSD Scan of FSPed region of 200 MPa sample and (b) Number fraction vs Misorientation angle plot of FSPed region 30
Fig. 5.5. Bar diagram comparing the relative densities of compacts before and after FSP .. 32
Fig. 5.6. Bar diagram comparing the average hardness values of all 7 samples before and after FSP 33
Fig. 5.7. Snapshot of the Tensile Specimen 34
Fig. 5.8. Stress vs Strain Curves for FSPed samples compacted at 7 different compaction pressures 35
Fig. 5.9. Bar diagram comparing the (a) UTS values and (b) Maximum Elongation values of FSPed samples compacted at 7 different compaction pressures 36
Fig. 5.10. Fractured surface of sample processed under conditions of 1525 rpm and 1 mm/min (a) compacted at 200 MPa (b) compacted at 250 MPa (c) compacted at 100 MPa and (d) compacted at 380 MPa 37
Fig. 5.11. Microstructure of (a) Green compact and (b) Sintered sample both compacted at 200 MPa and (c) Microstructure of the sample after FSP 38
Fig. 5.12. SEM images of (a) Green and (b) Sintered sample compacted at 200 MPa 39
Fig. 5.13. Bar diagram indicating the relative densities of samples before and after FSP ... 40
Fig. 5.14. Bar diagram comparing base and FSPed hardness of the 4 samples 42
Fig. 5.15. Stress vs strain curves for pure Al and Al-0.5%Mg green and sintered FSPed samples 43
Fig. 5.16. Bar diagram comparing the values of (a) UTS and (b) maximum elongation for the 4 FSPed samples 44
Fig. 5.17. Fractured surfaces of (a) green FSPed and (b) sintered FSPed samples both compacted at 200 MPa and processed under conditions of 1525 rpm and 1 mm/min 44

Fig. 5.18. Microstructure of (a) Al-10wt%Cu green compact and (b) Al-10wt%Cu FSPed sample 45
Fig. 5.19. EDS Analysis of FSPed region of Al-10wt% Cu sample 46
Fig. 5.20. EDS Mapping images showing (a) the area of observation (b) distribution of Al and (c) distribution of Cu in Al-10wt%Cu powder mixture 46
Fig. 5.21. EDS Analysis of Al-1wt%Cu sample 47
Fig. 5.22. EDS Analysis of Al-5wt%Cu showing the variation of Cu content as the region of selection is moved away from the light coloured region 47
Fig. 5.23. Bar diagram comparing the relative density values before and after FSP 49
Fig. 5.24. XRD pattern of Al-1wt%Cu sample before and after FSP 50
Fig. 5.25. XRD pattern of Al-5wt%Cu sample before and after FSP 50
Fig. 5.26. XRD pattern of Al-10wt%Cu sample before and after FSP 51
Fig. 5.27. XRD pattern of Al-Cu samples after FSP 51
Fig. 5.28. Bar diagram showing hardness values of Al-Cu samples along with pure Al before and after FSP 53
Fig. 5.29. Stress vs strain curves for Al-Cu FSPed samples along with Pure Al 54
Fig. 5.30. Comparision of (a) UTS and (b) Maximum Elongation values for all 4 samples 55
Fig. 5.31. Fractured surface of (a) Al-1wt%Cu FSPed sample and (b) Al-5wt%Cu FSPed sample (c) Fractured surface of Al-10wt%Cu FSPed sample and (d) Region of crack propagation through the intermetallic in case of Al-10%Cu FSPed sample 56

LIST OF TABLES

Table 1. Density Measurement of Green and FSPed samples 31
Table 2. Hardness Measurement of Base material and FSPed region 33
Table 3. Measurement of UTS and Maximum Elongation of 7 samples 35
Table 4. Density measurement of 200 MPa Green and Sintered Samples before and after FSP 40
Table 5. Hardness Measurement of Green, Sintered and FSPed 200 MPa compacted sample 41
Table 6. Measurement of UTS and Maximum Elongation 43
Table 7. Theoretical density values for various compositions 48
Table 8. Density measurement of Al-Cu samples and comparision with pure Al 48
Table 9. Hardness measurement of Al-Cu samples before and after FSP 52
Table 10. Measurement of UTS and Maximum Elongation of Al-Cu FSPed samples 54

Chapter 1 INTRODUCTION

1.1 Powder Metallurgy

Powder metallurgy (PM) [1] is a branch of metallurgy in which various components are manufactured from metal powders. It basically consists in mixing of fine powdered materials, compressing the powder to produce a green compact and then heating the green compact in a protective atmosphere to a temperature below the melting point of the metal. The final step of heating is known as sintering and this particular step helps in the development of proper bond between the powder particles which in turn renders the final powder metallurgical product sufficiently strong for the intended use. The strength of sintered products is much higher as compared to that of green compacts and it is these sintered products which are fit for practical applications [4,5].

The production of components via powder metallurgy route has many potential advantages when compared to producing them via conventional methods such as machining from billets. Powder metallurgy is a near net shape forming process and hence in many cases it does not require any finishing operation. The dimensional accuracy possible is very high. It also brings about flexibility in design. Products with intricate shapes can be easily manufactured through PM route. Out of all known manufacturing processes, it has the maximum material utilisation rate. Cost savings are made in powder metallurgy route. Not only these, flexibility to produce compositions not possible by other methods is an added advantage of PM.

The applications of powder metallurgy are very wide. Powder metallurgy products are present in hardware, washing machines, power tools, parts of automobiles, cutlery knives, X-ray shielding etc. The samples produced through powder metallurgy route contain porosities which can be highly reduced by using processes like-friction stir processing. As a result, the mechanical properties also get enhanced.

1.2 Friction Stir Processing

1.2.1 Introduction to Friction Stir Processing

Friction Stir Processing (FSP) was first developed by Mishra et al. [6,7,8] as a process for microstructural modifications and it works on the principles of friction stir welding (FSW).The working principle of FSW is very simple. It uses a non-consumable rotating tool with a pin at its head. The shoulder of the tool with its pin is inserted into the abutting edges of the plates to be joined and the tool is then traversed along the line of the joint. Heat is produced because of friction between the tool and the workpiece and as plastic deformation occurs it makes the workpiece material soft and a solid state welding is obtained.

1.2.2 Working Principle of Friction Stir Processing

Friction Stir Processing (FSP) is mainly a surface modification technique and is carried out by a specially designed non consumable tool. Generally a cylindrical tool with a pin at its head is used. The tool rotates about its axis and is plunged into the sample. As a result, the temperature of the workpiece rises which makes the material soft. The tool is then given a traverse feed along the length of the specimen. The primary functions of the tool are: (a) heating of workpiece due to the presence of friction between the tool and the material and (b) movement of material [8]. Due to localised heating, the material around the pin softens and a combination of tool rotation and translation leads to movement of material around the pin. The direction of material movement around the pin is quite complex. During FSP, the material undergoes intense plastic deformation at elevated temperatures which causes dynamic recrystallization to occur. As a result fine and equiaxed recrystallized grains are obtained in the processed zone.

1.2.3 Process Parameters

The processing parameters of Friction Stir Processing are- (a) tool geometry which includes the shoulder diameter, the pin diameter and the pin length (b) the tool rotation rate (R), (c) the tool traverse rate (v), (d) the angle of spindle or tool tilt and (e) the plunge depth of the pin.

The tool geometry plays a very crucial role in material flow. The relative size of the shoulder and the pin is very important aspect to consider from heating point of view. The initial heating results from the friction between the pin and the workpiece. The pin is

generally plunged till the shoulder touches the workpiece material. However its the friction between the shoulder and the work piece which provides the biggest component of heating. Hence, to obtain a defect free processed zone, a specific ratio should be maintained between the shoulder and pin diameter. For enhancement of the processed zone, different types of pin (threaded pin with flutes, threaded pin, cylindrical pin) are used as shown in Fig.1.1. (b) [8].

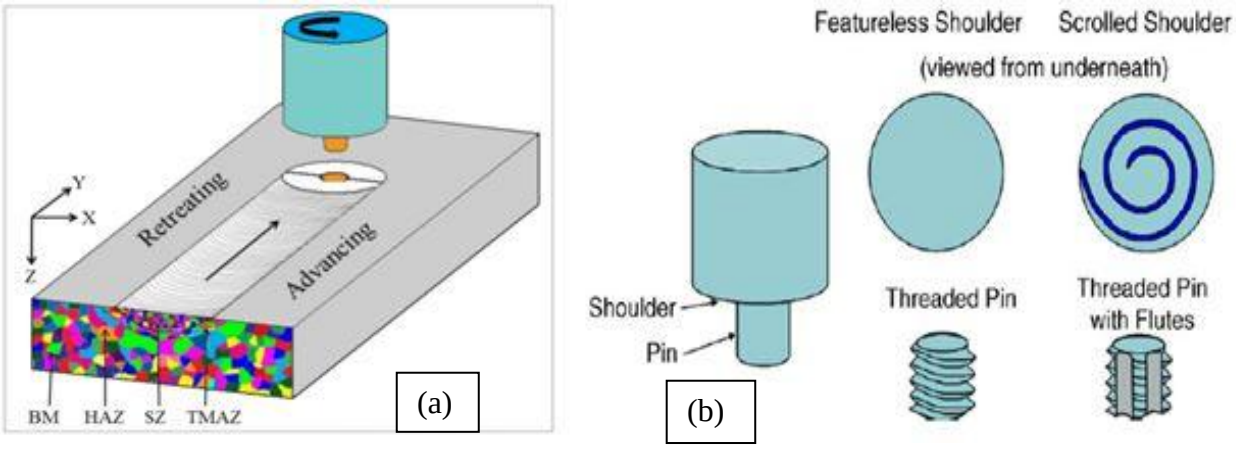

Fig. 1.1. (a) Schematic of FSP Process [12] and (b) Different pin designs of a FSP tool [8]

Another important factor which has a critical impact on the processing is the ratio of the tool rotation rate to the tool traverse rate (R/v). It gives a direct measure of the heat input into the workpiece [7,8]. The ratio should neither be too low nor should it be too high. If its too low, the heat generated would be insufficient for proper softening and hence the stirring and mixing of the material won't be fine. At the same time, if the ratio is too high, it will result in turbulent flow of the material which may cause cavities in the stir zone. In either of the cases, there will be defects present in the stir zone. Hence, an optimum value of the ratio is required for proper processing of the material.

In addition to the above, the angle of tool tilt also has an important impact. A suitable tilt of the spindle towards the trailing direction is necessary to ensure that the shoulder would hold the stirred material by the pin and move the material efficiently from the front to the back of the pin. The plunge depth of processing is also a key factor in FSP. A very low value of

it would result in inadequate forging whereas a value too high would result in material loss. The pin length determines the plunge depth of processing.

1.3 Metal Matrix Composites

Metal matrix composites (MMCs) [3] are a widely used class of material for structural and electrical applications. They can be produced by a variety of processing routes like powder metallurgy, ultrasonic solidification, mechanical alloying etc. The MMCs can be sub divided into several categories but out of these the particulate reinforced MMCs are of primary interest. This is because of their easy fabrication along with high strength, low cost, low weight and isotropic properties. The particulate reinforced MMCs have high strength and low weight primarily because of the existence of in-situ reinforcements. The conventionally PM processed MMCs [2] have certain drawbacks. The amount of reinforcing phase is restricted by the initial powder size and the in-situ reinforcements also grow in size during sintering which results in poor mechanical properties. In addition to these, the presence of porosities, reduced interfacial bonding and wettability between the matrix and reinforcement due to reinforcement contamination are some other major drawbacks. Hence, synthesis of in-situ reinforcement is desired so that the bonding between the matrix and the reinforcement is increased considerably. This can be achieved by using a surface modification technique called Friction Stir Processing (FSP).

Aluminium is the one of the most used matrix material for the metal matrix composites (MMCs) [3]. The Al alloys are very useful mainly because of their low density, high thermal and electrical conductivity, high damping capacity and good corrosion resistance. These alloys offer a large variety of mechanical properties and it depends on the chemical composition of the Al-matrix. They can be primarily classified into two categories namely: casting alloys and wrought alloys. It has been found that around 85% of aluminium is used for wrought products. Aluminium alloys are very widely used in manufacture of aircrafts due to their high strength to weight ratio. But pure aluminium has very limited use as it is very soft and does not possess sufficient tensile strength to be used in helicopters and aircrafts. Copper has been one of the most studied alloying elements added in the aluminium metal matrix composites. In case of cast alloys the basic structure is dendritic in nature and possess aluminium solid solution along with particles of varied nature at the grain boundaries or interdendritic spaces which forms brittle components with eutectics in nature. Most of the alloying elements can improve the modulus of elasticity of aluminium but this increase is not remarkable for the aluminium-copper alloys. The modulus of

elasticity at room temperature for such an alloy is in the range of 70-75 GPa and is almost the same in compression and in tension. It shows a uniform variation with temperature from a value of 76-78 GPa at 70 K to a value typically of the order of 60 GPa at 500 K. The Poisson ratio is typically of the order of 0.32-0.34. The Poisson ratio also increases with increasing temperature [3]. Many of the cast alloys and aluminium-copper-nickel alloys are used widely for high temperature applications where creep resistance is a crucial consideration [3].

The desirable properties of Metal Matrix Composites (MMCs) mainly arises due to the presence of small, high strength ceramic particles which are distributed uniformly throughout the aluminium alloy matrix. It has been found that the aluminium MMC castings are economically quite competitive with iron and steel castings. However, the machining cost is a bit high in case of aluminium alloys due to its low machinability. The reason for low machinability is the presence of the wear resistant ceramic particles. As a result, cast MMCs find limited application to components which require a large amount of secondary machining.

FSP has been primarily utilised to refine the microstructure of different metal matrix composite and enhance mechanical properties [15]. Due to the stirring action of the tool and the heat produced as a result of the friction between the tool and the material, the material becomes soft. Hence, the material movement takes place. Plastic deformation is achieved and recrystallization occurs. A homogenised fully dense solid is formed along with the in situ intermetallic phase [24]. The Orowan strengthening from this nanosized intermetallic phase, grain boundary strengthening and the load sharing effect of the reinforcements contribute to the high composite strength [24].

Discontinuously reinforced metal matrix composites (MMCs) have found considerable use in many sectors. The primary reasons for this are: (a) ready availability of various types of reinforcement at reasonable costs (b) successful development of manufacturing processes for producing Metal Matrix Composites which show reproducible properties and (c) the availability of metal working methods that can be used to produce these MMCs [16]. These MMCs are fabricated in mainly two ways. They are fabricated either by direct addition of reinforcements into the matrix or sometimes the reinforcements are synthesized in situ in the metal matrix [16,17,18].

There are some advantages of in situ MMCs. They are thermodynamically more stable, their microstructure is also more homogeneous and they also have strong interfacial bonding between the matrix and the reinforcement [25].

Friction Stir Processing (FSP) leads to formation of certain in situ composites. One such example is the formation of in situ Al-Al_2Cu composite [24]. The application of FSP leads to the formation of in situ Al–Al_2Cu composite and the main reason behind it is the hot working nature of FSP. In short, FSP can provide (a) severe plastic deformation which facilitates proper mixing and material movement, (b) elevated temperature to promote the formation of an intermetallic phase and (c) hot consolidation resulting in a fully dense solid.

2.1 Macrostructural and microstructural evolution during FSP

FSP results in reduction of defects such as-porosities, inhomogeneity etc to a large extent in cast as well as sintered material. As the rotating tool with the pin is plunged into the specimen, heat is generated due to friction between the tool and the material. As a result, the material around the pin softens and material movement takes place. Intense plastic deformation is achieved and recrystallization occurs which results in formation of new grains. FSP results in fine microstructure which leads to highly enhanced mechanical properties [8]. In FSP, two terms are very commonly used i.e the advancing side and the retreating side. The advancing side is the side on which the tangent to the rotating tool and the direction of traverse movement are same and the retreating side is the side at the diametrically opposite end. On the basis of the metal working processes, the region of FSP can be basically sub-divided into five zones namely: (a) preheat (b) initial deformation (c) extrusion (d) forging and (e) post heat/cool down. The preheat zone is the zone just in front of the traversing tool. The combination of rotational and traverse movement of the tool deforms the material plastically and helps in the flow of material from the front to the back of the pin. The material which flows to the back of the pin is extruded and forged into the cavity which is left behind by the tool. In this manner a consolidated microstructure is obtained.

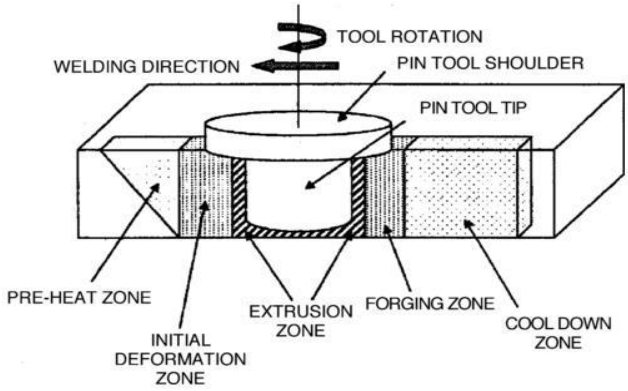

Fig. 2.1. Metallurgical processing zones developed during FSP [8]

In the study of microstructure of friction stir processed regions of 6061Al and 7075Al alloys, Krishnan et. al.[10] confirmed that FSP can be linked to an extrusion process. Ma et. al.[9] conducted a study on the microstructural modifications that occurred through FSP in cast A356 alloy. It was found that at low rotation speeds, the processed zone (nugget) takes basin shape and with increase in speed it gradually changes to elliptical shape. This is because with increase in speed, the stirring action of the rotating tool is greater and the temperature gradient is higher. The nugget zone acquires onion shape as the tool rotation attains a speed of about 800 rpm [8,9]. In the nugget zone, the strain energy associated with plastic deformation is sufficient for recrystallization to take place. Hence we obtain fine and equiaxed recrystallized grains in this particular zone. It has been found that the dislocation density is relatively low in the interior of the recrystallized grains [8]. However, some researchers have reported that these grains contain high density of sub- boundaries [8], subgrains [8] and dislocations. Just adjacent to the nugget zone lies the thermo-mechanically affected zone (TMAZ) [8,9]. In this zone, plastic deformation takes place but recrystallization does not occur due to insufficient deformation strain. However, it was observed that there was dissolution of precipitates in the TMAZ. The grains in the TMAZ are generally elongated in shape and contain high density of sub-boundaries [9]. Finally, beyond the TMAZ, there is the heat affected zone (HAZ). In this particular zone, the material experiences a thermal cycle but it does not undergo any plastic deformation. Mahoney et. al. [6] defined HAZ as a zone which experiences a temperature rise above 250°C for a heat treatable Al alloy. The structure of the grains in the HAZ are generally the same as that of the parent material.

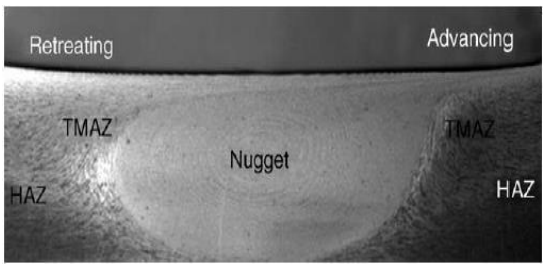

Fig. 2.2. A typical macrograph highlighting different the different microstructural zones in FSP 7075Al [8].

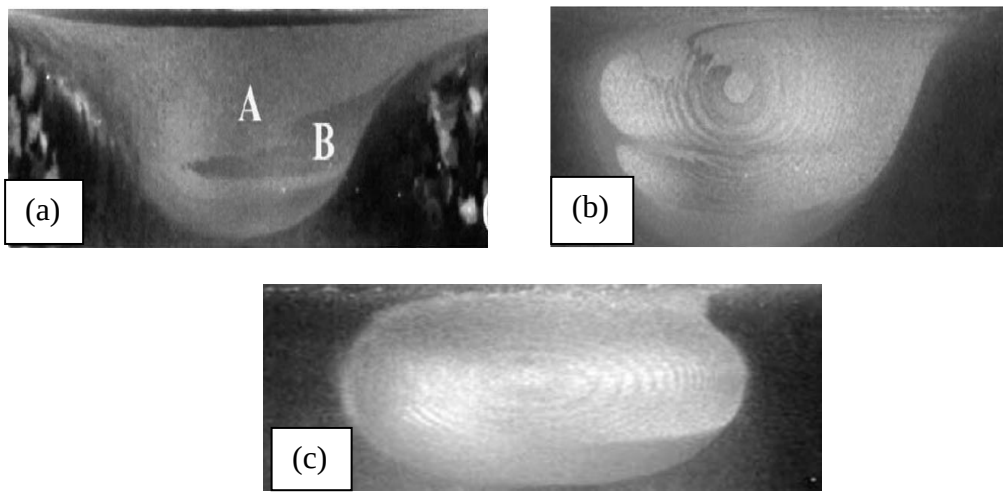

Fig. 2.3. Variation in shape of stir zone with processing parameter in FSP A356 (a) basin shaped, 300 rpm/51 mm/min (b) elliptical, 700 rpm/102 mm/min(c) onion shaped, 900 rpm/203 mm/min [9]

2.2 Recrystallization Mechanisms

It is well accepted that dynamic recrystallization is the mechanism responsible behind the generation of fine and equiaxed grains in the nugget zone during FSP. The process parameters, composition of workpiece, temperature of workpiece, vertical pressure and active cooling are the main factors affecting the size of recrystallized grains during FSP. Researchers have proposed several mechanisms for dynamic recrystallization process in aluminium which includes- discontinuous dynamic recrystallization (DDRX), continuous dynamic recrystallization (CDRX) and geometric dynamic recrystallization (GDRX). Aluminium and its alloys generally do not experience DDRX because of their high rate of recovery which is a result of aluminium's high stacking fault energy [11]. Jata and Semiatin [13] were the ones who were first to propose that CDRX is the operative nucleation mechanism during FSP. According to them low angle boundaries present in the parent metal are replaced by high angle boundaries in the nugget zone after FSP. This occurs by means of continuous rotation of the original low angle boundaries. Not only these, it was also observed that many of the recrystallized grains in the stir zone are finer than the original subgrain size. Thus it is very less likely that the recrystallized grains in the stir zone are a result of rotation of original elongated subgrains in the parent metal. According to Su et al. [14], dynamic recrystallization in the nugget (stir) zone can be considered a CDRX based on the phenomenon of dynamic recovery. But there is also a contradiction to this. As the recrystallized grains in the nugget zone of FSP aluminium alloys are considerably

smaller than the pre-existing subgrains in the parent alloy, so from this it can be strongly suggested that DDRX is the operative mechanism for recrystallization. So, the exact operative mechanism of recrystallization during FSP cannot be certainly ascertained. However, by minutely observing the microstructure of the stir zone after performing FSP, we can get an idea about whether CDRX or DDRX is the main recrystallization mechanism during FSP on powder sample.

2.3 Effect of process parameters on grain size

The size of the recrystallized grains can be reduced by decreasing the tool rotation rate and keeping the tool traverse speed constant. Moreover, decreasing the ratio of the tool rotation rate to the traverse speed also reduces the grain size. This is because under these conditions, the flow stress is higher and hence the grains do not have a tendency to grow, instead they get fragmented. However, as the ratio is increased, more amount of heat is generated and as a result the diffusivity and growth of grains becomes easier because of which larger grains are obtained.

This dependency of the grain size on the strain rate and temperature can be summarized in terms of Zener-Holloman parameter (Z) [20]. Z is given by the following equation-

$$Z = \mathcal{E}\, exp^{\frac{Q}{RT}} \qquad (1)$$

where $\mathcal{E}$ gives the strain rate, Q is the activation energy, R is the gas constant and T is the temperature attained.

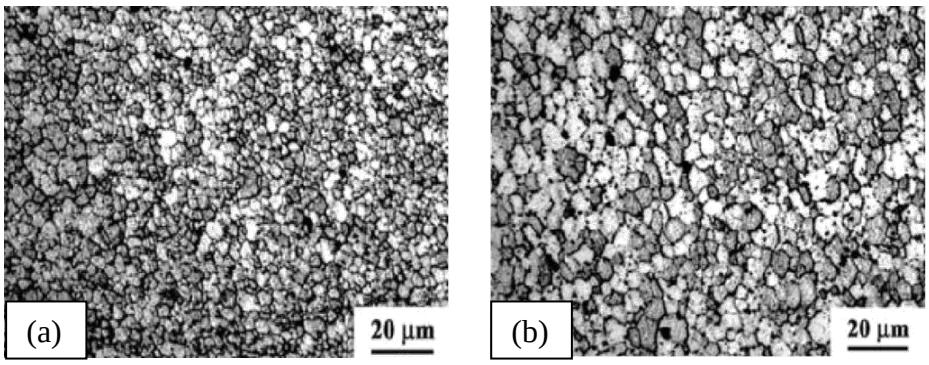

Fig. 2.4. Effect of FSP process parameters on grain size of nugget zone in FSPed 7075Al at (a) 350 rpm, 152 mm/min and (b) 400 rpm, 102 mm/min [19].

At low values of Z (low strain rate and high temperature), there occurs an increase in the grain size as well as the volume fraction of the dynamically recrystallized grains. Whereas at high Z values i.e when the strain factor is dominant, just the opposite happens. Kwon et al [34] studied the effect of rotational speed on grain size. He observed that as the rotational speed was increased from 560 rpm to 1840 rpm at constant traverse speed of 155 mm/min, the grain size also gradually increased from 0.5µm to 4 µm. In the study of FSP of 7075 Al alloy it was observed that on decreasing the ratio of tool rotation/traverse speed from 400 rpm/102 mm/min to 350 rpm/152 mm/min, the recrystallized grain size also decreased from 7.5 to 3.8 µm [19]. Bauri et al. [15] performed FSP on pure Al powder using tool rotation rate of 640 rpm and traverse speed of 150 mm/min and observed a reduction in grain size from 84 µm to 3µm. He suggested that 640/150 was the minimum ratio of tool rotation to traverse speed that could be used to obtain a defect free stir zone. However, the interesting thing is that with the increase in the tool rotation rate, both strain rate and the peak temperature in the thermal cycle of the processed zone increases. While higher temperature results in higher size of the recrystallized grains and grain growth, strain rate makes the grains finer. Thus it is the relative dominance of the strain factor over the temperature or vice versa that determines the microstructure of the material. Hence from the observation of mechanical properties, there must be an optimum ratio of rotational speed to traverse speed. The temperature which is attained during processing must be high enough for the nugget to enter soft and recrystallized zone but at the same time it must be moderate enough to avoid grain growth. It was also found that by addition of reinforcements and increasing the number of passes, grain size decreases due to pinning action on the grains [9].

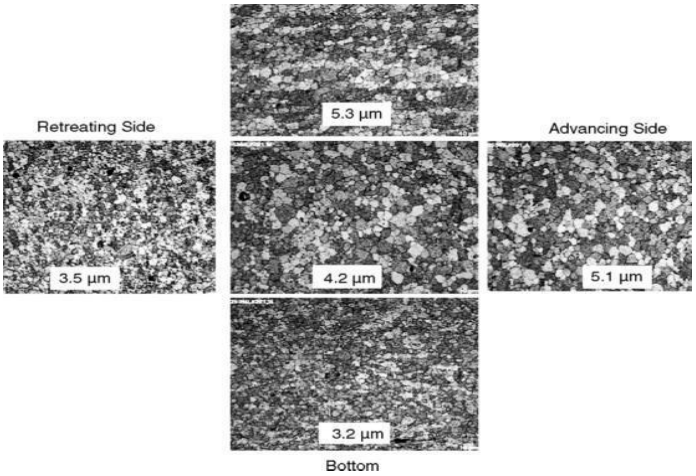

Fig. 2.5. Distribution of grain size in various sections of 7075Al weld nugget [19].

2.4 Applications of friction stir processing on metal matrix composites fabricated through powder metallurgy route

Friction stir processing is a useful surface modification technique which helps in enhancing the properties of metal matrix composites. This is by virtue of refinement of grains in the microstructure of the composite. This process mainly utilises the heat produced due to friction between the tool and the workpiece and also the plastic deformation of the workpiece. After FSP, a fully homogenised dense solid is obtained along with an in situ intermetallic phase. The Orowan strengthening resulting from the nanosized intermetallic phases, grain boundary strengthening and the load sharing effect of the reinforcements are the primary contributors to high composite strength.

Kao et al. [24] studied the effect of FSP on Al composite. The composite consisted of Al and Cu powders which were compacted and then sintered. It was found after FSP an in situ intermetallic phase Al_2Cu was formed. These intermetallics synthesized are distributed intragranularly, resisting movement of dislocations and thus have a restraining action on the matrix grain size. This resulted in increase in hardness value to almost two times of that of the sintered compact. Not only this, the yield strength (YS), ultimate tensile strength (UTS) were also enhanced significantly after FSP. The composite also showed a reasonably good compressive ductility. Similar kind of work had also been carried out by Kao et al. [2] on Al and Ti mixture. In this case, the reinforcement formed was Al_3Ti. During study on this mixture, the rotational speed, the number of FSP passes and the Ti content was varied. It was found that at low rpm, the strength values increased with increasing number of passes and also with increase in Ti content. Kao et al. [26] has also reported similar enhancements in mechanical properties in the composite formed out of Al and Fe powders. Kao et al. [35] have done considerable work on Al-Si sintered powder composite and has improved upon the mechanical properties in the Al-SiO_2 mixture [27]. Kao et al. [28] has also studied on Al-CeO_2 mixture. However, in this case, the tool traverse speed and the sintering temperature was varied. It was observed that the strength values decreased with the increase in the traverse speed. At a specific sintering temperature (833K), the reaction between Al and CeO_2 to form the reinforcements $Al_{11}Ce_3$ and delta-Al_2O_3 was complete and it gave the highest strength. As the heat of formation of the reaction was very high, so FSP was carried out at a low rpm. Kao et al. [29] also carried out FSP on Al-TiO_2 sintered mixture in which the heat of formation of Al_3Ti was comparatively lower. Hence the growth of Al_3Ti could be effectively controlled even at higher rpm giving higher ductility. Kao et. al.[30] have

investigated on Al/CuO powder mixture and found that due to dispersion of the nanosized Al_2Cu and Al_2O_3 particles, the strength and ductility of the composite was greatly enhanced. From TEM imaging it was evident that the Al_2O_3 particles are formed between the Al and CuO core and this in turn limited the formation of Al_2Cu. Hence, Kao et. al.[31] suggested the addition of Mg powders in the sintered mixture. This is because stable MgO forms and Cu particle getting reduced undergo reaction with aluminium to form the reinforcement Al_2Cu. This in turn resulted in higher strength values. Ma et. al.[32] had an idea of homogenising the CNT distribution in Al matrix. For this purpose, they carried out FSP. The results of Raman spectroscopy showed the retention of layered structure of the CNTs even after FSP although they were shortened. The Yield Strength and the Ultimate Tensile Strength were found to increase. The yield strength showed a uniform increase with increase in CNT concentration but the UTS showed a decreasing trend. The study of the same composite at elevated temperatures was also carried out by Ma et. al.[33].Coefficient of thermal expansion was observed to decrease with increase in the CNT concentration after FSP and this makes the composite suitable for high temperature application. Izadi et. al.[36] carried out FSP on Al-SiC composite after sintering. It was seen that the presence of small size and high volume fraction of SiC particles resulted in greater surface area of friction and this led to pretty high initial porosity in the as sintered material which could not be completely consolidated by FSP.

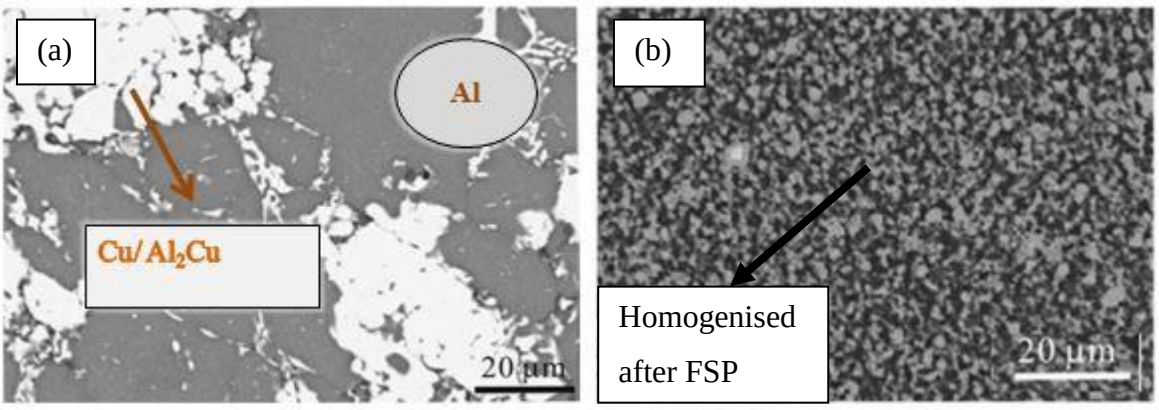

Fig. 2.6. SEM Image of (a) Al- 15 %Cu sintered at 803 K (b) Al- 15 %Cu sintered at 803K followed by 2 FSP passes [24].

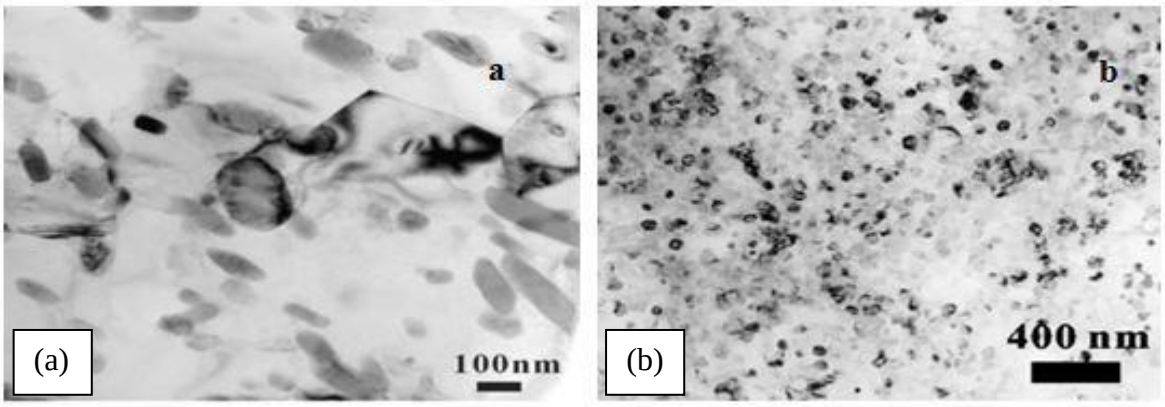

Fig. 2.7. (a) Fine $Al_{13}Fe_4$ [26] and (b) Fine Al_3Ti [2] particles uniformly distributed in aluminium matrix.

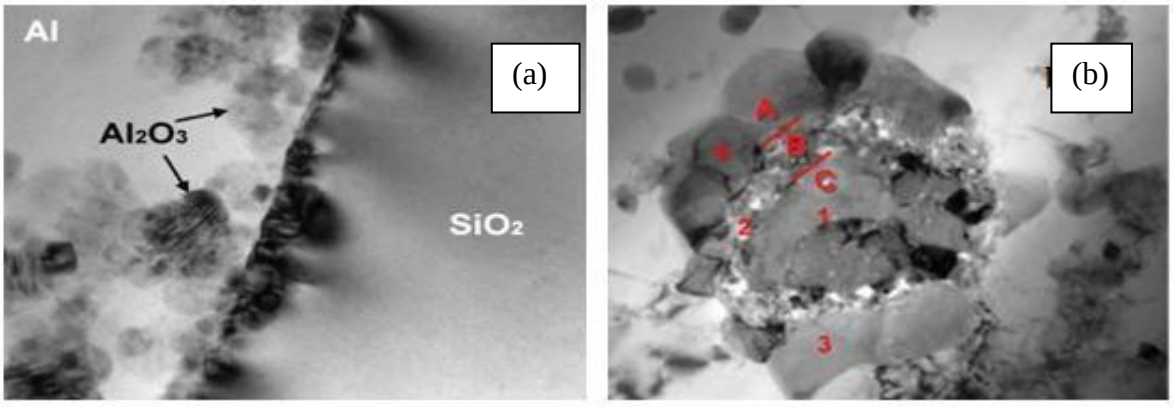

Fig. 2.8. TEM/BFI Image showing the formation of (a) Al_2O_3 particle at the Al/SiO_2 interface [27] and (b) CuO/Cu_2O (C), enclosed by a shell comprised of aluminium oxide (B) and Al_2Cu (A) in FSPed Al–10CuO specimen [30].

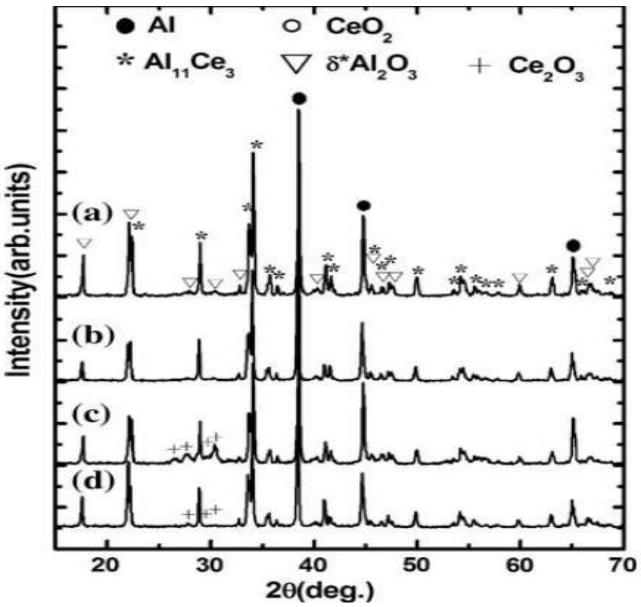

Fig. 2.9. XRD patterns of FSPed Al- CeO_2 composite processed using different tool traversing speeds. The FSP was performed (sintered at 883K) with a tool rotating rate of 500 rpm and traverse speed of (a) 30 mm/min (b) 85 mm/min or (c) 120 mm/min. (d) Specimen was sintered at 813 K followed by four FSP passes with parameters, 500 rpm and 30 mm/min [28].

2.5 Strengthening mechanisms in Friction Stir Processed composites

FSP is basically used as a tool for enhancing the mechanical properties of metal matrix composites primarily by refinement of microstructure of the composite. During FSP, due to intense plastic deformation occurring at elevated temperatures, some in situ intermetallics are formed. The main strengthening mechanisms which come into play during FSP are- Orowan strengthening which results from nanosized intermetallic phase, grain boundary strengthening due to refinement of grains and solid solution strengthening. Besides, in case of composites, the load sharing effect due to addition of reinforcements also contribute significantly to high composite strength.

Orowan strengthening results from the intragranular interaction between the nano-sized intermetallic particles with the dislocations. This interaction hinders the movement of the dislocations thereby enhancing the strength of the composite. The equation for Orowan strengthening [2] is given by equation 2:

$$\tau_{OR}=\frac{0.81\,Gb}{2\pi(1-\nu)^{1/2}\,\lambda}\ln\left(2\sqrt{\frac{\frac{2}{3r}}{r_0}}\right) \quad (2)$$

where G is the matrix shear modulus, b is the Burgers vector, ν is Poisson's ratio, and r_o (=4b) is the dislocation core radius, and λ is the interparticle spacing. It has been observed that on increasing the reinforcement content, there is a rise in the Orowan strengthening effect.

The grain boundary strengthening basically results from the refinement of the grains. It is based on the Hall Petch equation. The Hall Petch equation can be written as-

$$\sigma_y = \sigma_0 + \frac{k}{\sqrt{d}} \quad (3)$$

where σ_y is the yield stress, σ_0 is a materials constant, k is the strengthening constant and d is the average grain diameter

The solid solution strengthening is the strengthening mechanism where the strength increases by virtue of addition of atoms of one element into the crystal lattice of another element. The alloying element diffuses into the matrix of base metal forming the solid solution. Solute atoms are either smaller or larger in size than the solvent atoms of a solid solution. Smaller atoms produce local tensile stress field while larger atoms produce local compressive stress field in the crystal. In both cases the stress field of the moving dislocation interacts with the stress field of the solute atoms. This increases the stress required to move the dislocation and hence results in increase in strength.

In FSP, it has been seen that if the ratio of the rotational speed to traverse speed is increased, the flow stress decreases. In such cases, the grains do not fragment readily and they grow in size with the increase in the ratio. However, it has also been seen that with higher rotating speed, the strain rate also increases and as a result the grains may refine as well depending on the dominance of strain rate over temperature attained. Thus we can say that the rotational to traverse speed ratio also has a huge influence on composite strength.

The Halpin– Tsai equation [3] is the basis for the load sharing effect in case of composites. The Young's modulus of elasticity increases uniformly with increase in the amount of reinforcement content for a composite.

$$\mathbf{E_c} = \frac{\mathrm{Em}(1+\eta q V)}{1-qV} \tag{4}$$

E_m, E_c and Ep are the Young's moduli of the matrix, composite and reinforcement respectively, η is an adjustable parameter, and V is the volume fraction of the particles.

$$\mathbf{q} = \frac{(\frac{\mathrm{Ep}}{\mathrm{Em}})-1}{(\frac{\mathrm{Ep}}{\mathrm{Em}})+\eta} \tag{5}$$

2.6 Gap in work and objective of my work

From the literature survey, it was found that FSP has not yet been tried on green compacts. So the main objectives of my work were as below:

1) To find out whether FSP is feasible on green compacts.

2) If it is feasible, then the mechanical properties are to be studied and microstructural characterization to be done.

3) To compare the results by performing FSP on sintered samples and to conclude whether the sintering step can be eliminated.

4) To study the effect of addition of alloying elements like copper to aluminium matrix and the compounds formed due to reaction between these elements during FSP.

Chapter 3 PLAN OF WORK

It is well known that the components prepared through powder metallurgy route are widely used in various automobile and machining parts. But there are some drawbacks of powder metallurgy products one of which is the presence of porosities and improper consolidation in some cases. In the current study, Friction Stir Processing (FSP), which is a surface modification technique in which plastic deformation occurs at elevated temperatures, has been applied to get rid of such drawbacks. The work that has been carried out can be sub-divided into three stages:

Stage I: Study the effect of compaction pressure on FSP and selection of the compaction pressure most suitable for FSP on PM sample

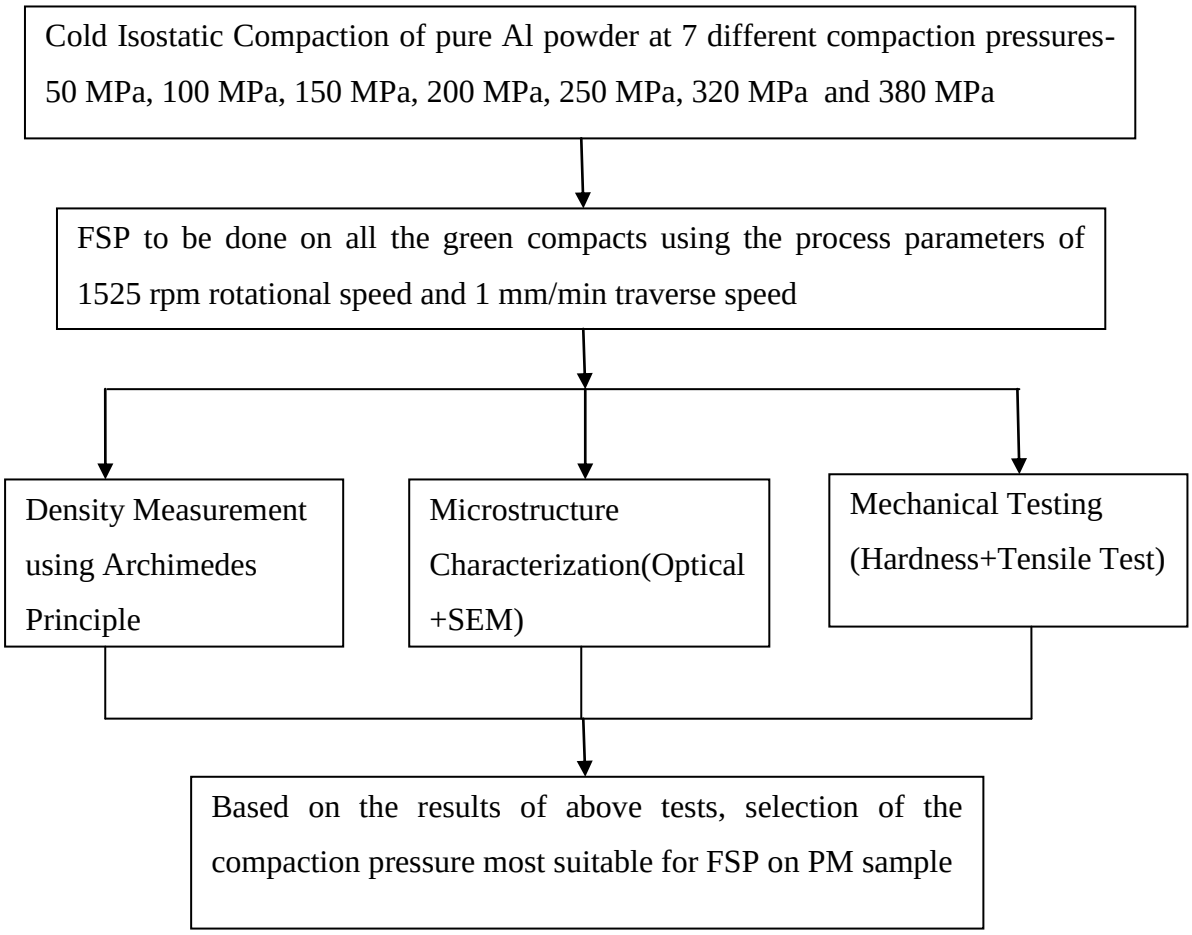

Fig.3.1. Flow diagram showing the work plan for determining the optimum compaction pressure

Stage II: Comparision between Green FSPed and Sintered FSPed samples compacted at 200 MPa

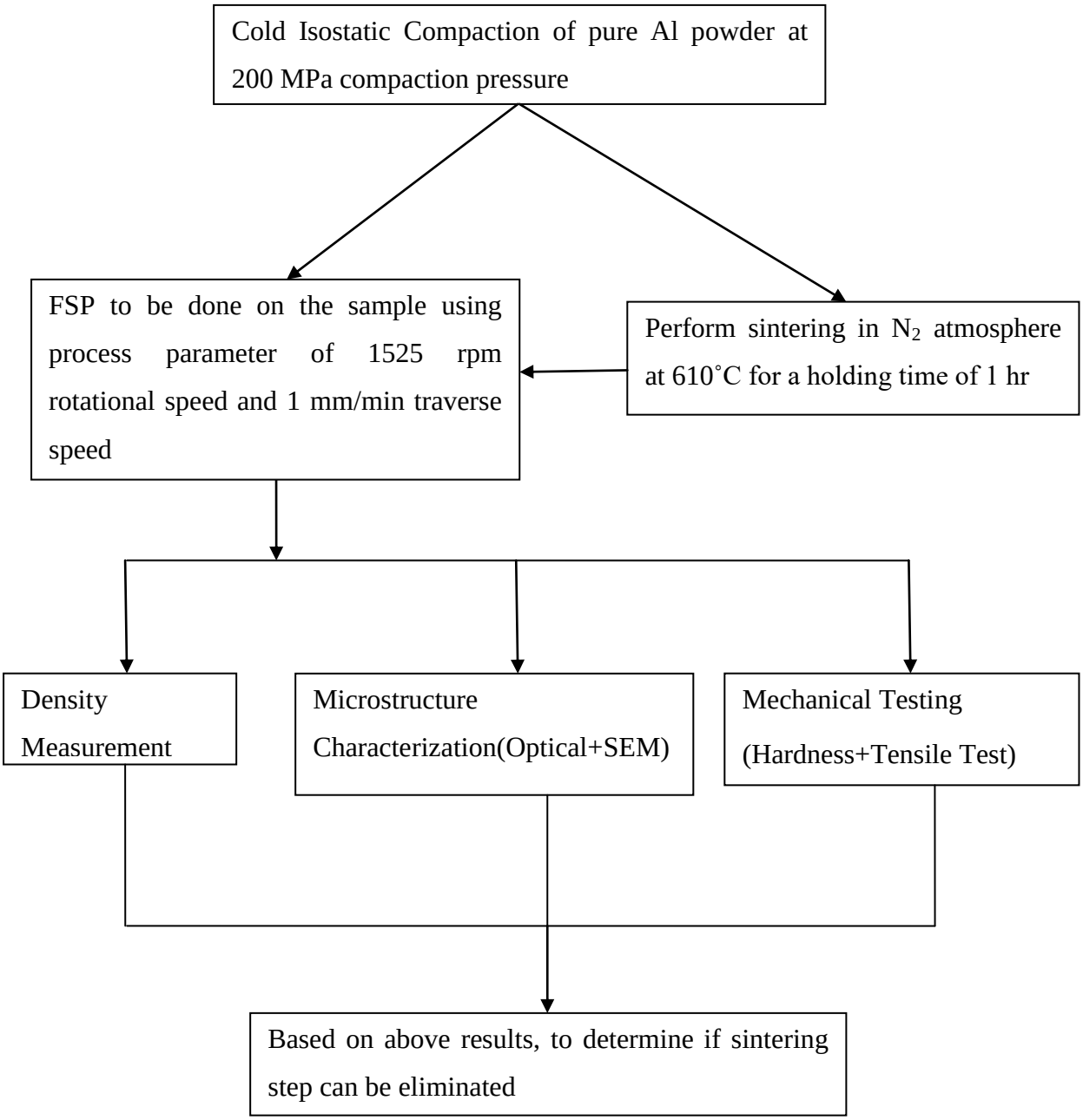

Fig.3.2. Flow diagram showing the work plan for comparision between green FSPed and sintered FSPed samples compacted at 200 MPa

Stage III: Study the effect of addition of Copper in Aluminium Matrix

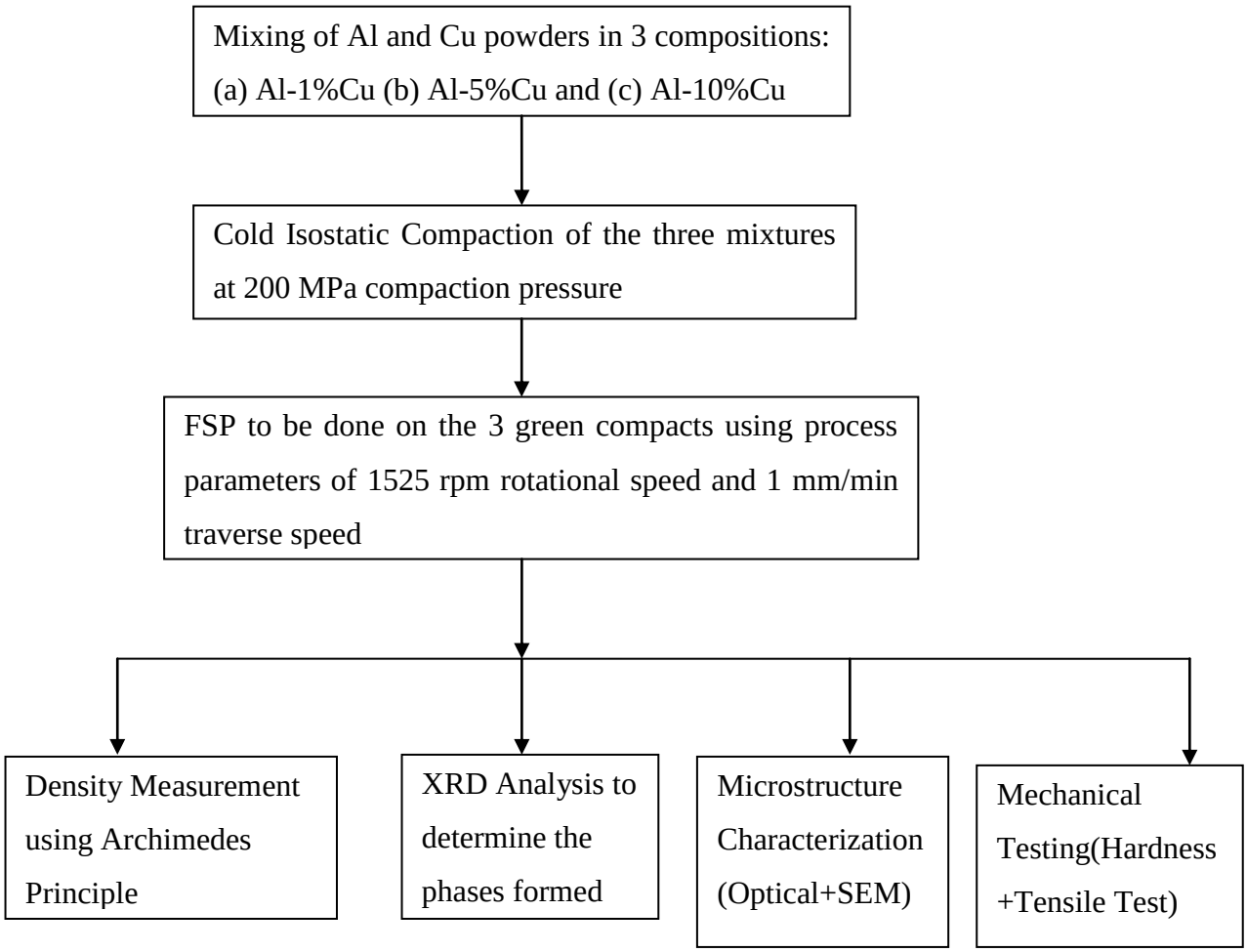

Fig. 3.3. Flow diagram showing the plan of work for determining the effect of copper addition into aluminium matrix

Chapter 4 EXPERIMENTAL PROCEDURE

4.1 Raw Materials Used

Aluminium metal powder having 99.9% purity with a mesh size of 325 and copper powder having 99.9% purity with the same mesh size of 325 were used as the raw material. Ultrafine nitrogen gas was used for sintering purpose.

4.2 Cold Isostatic Compaction

4.2.1 Pure Aluminium Sample

The samples to be used for processing were prepared using the powder metallurgy route. First of all, pure Aluminium powder was filled in a mould made of hard rubber having dimensions 80mm x 50mm x 15mm. The mould was then tightly packed from outside using a black tape in order to make it waterproof. Green compacts were then prepared by using the cold isostatic press (CIP) machine which is shown in Fig.4.1. Compaction was done at seven different pressures-50MPa, 100MPa, 150MPa, 200 MPa, 250MPa, 320MPa, 380MPa. These green samples were then used for performing FSP.

4.2.2 Al-Cu Sample

In this case also, the samples were prepared using the powder metallurgy route. The pure aluminium and copper powders were first of all thoroughly mixed in a ball milling machine. Almost 300g of Al-Cu powder was used up in the process of preparation of a single sample. The Al-Cu powder were mixed in 3 different proportions i.e Al-1%Cu, Al-5%Cu and Al-10%Cu. During mixing toluene was also used so that the powder doesn't stick to the balls. The mixing was allowed to continue for 6 hours. After that the mixture was taken out from the machine and allowed to dry for 2 hours. The completely dried powder mixture was then poured into the rubber mould having dimensions 80mmx 50mmx 15mm. The mould was tightly packed from outside using black tape. Compaction was then done at 200 MPa compaction pressure for the 3 powder mixtures of Al-1%Cu, Al-5%Cu and Al-10%Cu. The green compacts thus obtained were then used for performing FSP.

Fig. 4.1. Cold Isostatic Press (CIP) Machine

4.3 Friction Stir Processing

Friction Stir Processing (FSP) was to be carried out on the green compacts. The FSP machine consisted of 8 different rotating speeds of the spindle. There is a belt plus gear mechanism which is used to change the speed as and when required. There is a semi automatic adjustable table which is for controlling the traverse movement as well as the plunge depth of the tool. The tool used for performing FSP had the specifications- shoulder diameter 22 mm, pin diameter 6 mm and pin length 2.5mm. The set-up of the FSP machine and the tool used is shown in Fig.4.2.(a) and Fig.4.2.(b) respectively:

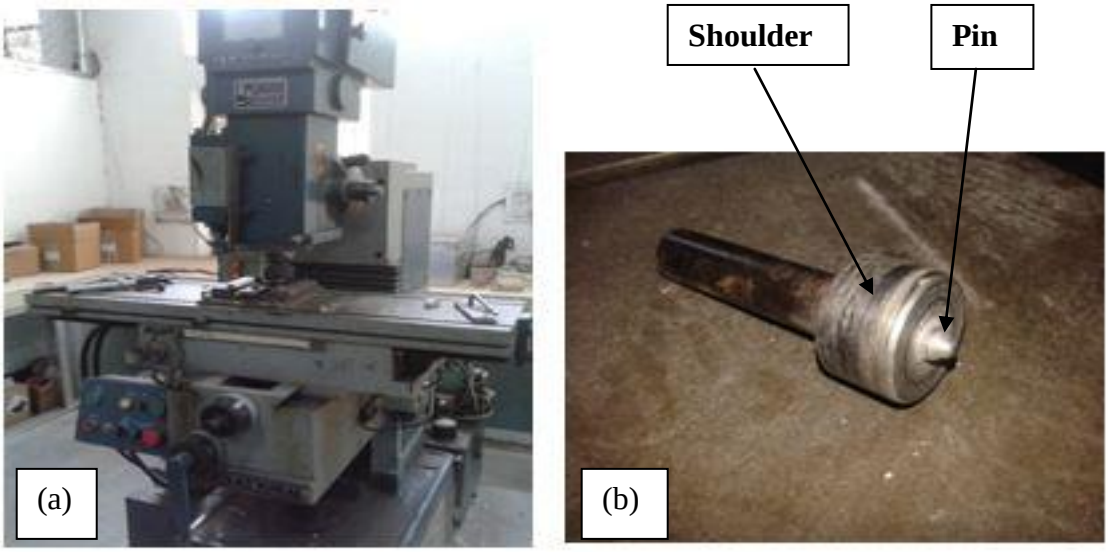

Fig. 4.2. (a) Friction Stir Processing Machine and (b) FSP tool

The ratio of the tool rotation rate to the tool traverse speed is a very important factor in FSP. It is a direct measure of the heat input to the sample. Before starting FSP, a small hole of 6 mm diameter and 2.5mm depth was made with a 6 mm drill bit on the starting plunging position. The tool holder and the fixtures used during processing of the sample is shown in Fig.4.3.(a). It is to be noted that the fixtures used were of adjustable nature and it did not depend on the dimensions of the sample although there was a limit to the maximum dimensions of the sample that could be processed. FSP was carried out on all the green samples compacted at 7 different pressures using the processing parameter of 1525 rotational speed and 1mm/min traverse speed. Holding time at the starting point of FSP was around 10 minutes. A processed sample using the above parameters is shown in Fig.4.3.(b). FSP was performed on the green as well as sintered Al-0.5% Mg sample using the same process parameters. In case of FSP of the Al-Cu samples also the process parameters used were- rotational speed of 1525 rpm and traverse speed of 1mm/min.

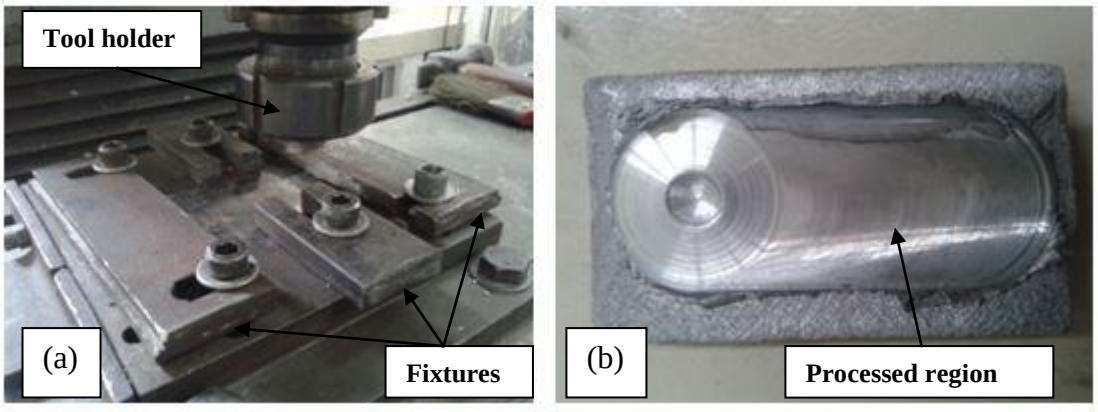

Fig. 4.3. (a) Tool holder and fixture used during processing (b) A FSPed sample using process parameters as 1525rpm and 1 mm/min

4.3.1 Selection of most suitable compaction pressure

FSP was performed on all pure Al samples compacted at seven different compaction pressures of 50 MPa, 100 MPa, 150 MPa, 200 MPa, 250 MPa, 320 MPa and 380 MPa. The FSPed samples were then analysed through microstructure characterisation and mechanical testing. Based on the enhancement of mechanical properties in the stir zone after FSP, the sample compacted at 200 MPa pressure was showing the best results. So 200 MPa compaction pressure was selected for further experiments. Then comparision was done

between properties of green and sintered FSPed samples compacted at 200 MPa. For proper sintering 0.5% of Mg was also added to pure Al.

4.3.2 FSP on Al-Cu composites for 3 different compositions

The effect of varying the concentration of copper in aluminium was intended to be studied. So Al-Cu samples were prepared via powder metallurgy route for 3 different compositions i.e Al-1%Cu, Al-5%Cu and Al-10%Cu at the selected compaction pressure of 200 MPa. Then FSP was performed on all the samples using process parameters of 1525 rpm and 1 mm/min rotational speed. After that microstructure characterisation and mechanical testing was done for each sample.

4.4 Porosity Calculation

The densities of the green compacts and that of the FSPed samples were measured using the Archimedes principle setup. For measuring the weights of the samples in water, distilled water was used. The porosity calculations were done by comparision of the calculated density with the theoretical density. The numerical relation for porosity calculation can be written as below-

$$\textbf{Porosity Percentage} = \frac{Theoretical\ Density - Calculated\ Density}{Theoretical\ Density} x100 \qquad (6)$$

4.5 Microstructure Characterization

For characterisation of the microstructure, transverse section of the FSPed samples were cut off. The samples were then polished using emery papers of different grades like-P320, P800, P1200, P1500 and P2000. It was followed by cloth polishing by using fine cloth with a slurry of MgO. Keller's reagent was used as the etchant. Buehler Simplimet 1000 automatic press shown in Fig.4.4.(a) was used to hot mount the samples before start of polishing in case of small samples. One of such mounted samples is shown in Fig.4.4.(b):

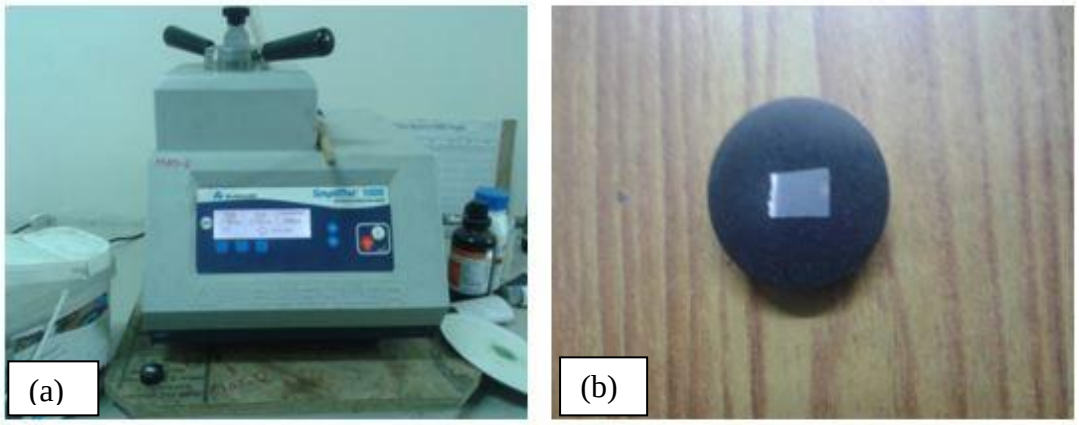

Fig. 4.4. (a) Buehler Simplimet 1000 automatic press and (b) A hot mounted sample

Optical microscopy (LEICA, MODEL:5000M) was carried out on the etched samples using the machine shown in Fig.4.5. For studying the distribution of elements in case of Al-Cu samples, energy dispersive spectroscopy (EDS) was carried out in scanning electron microscope (ZEISS).The scanning electron microscope (SEM) used is shown in Fig.4.6. Fractography was also carried out in SEM for the fracture analysis of tensile specimen. It gave us an idea of the nature of the fracture- brittle or ductile or both. The point of origin of the crack could also be ascertained which helped to find out the cause of crack initiation and subsequent failure.

Energy back scattered diffraction (EBSD) was performed on the pure Al sample compacted at 200 MPa after FSP in order to determine the reduction in grain size due to FSP and also the grain boundary orientation. During sample preparation for EBSD in addition to paper and cloth polishing, the sample was also polished using colloidal silica gel after which it was electro-polished using a solution of 80% methanol and 20% perchloric acid. During electropolishing, the voltage used was 12 V.

Fig. 4.5. Optical microscope (LEICA,5000M)

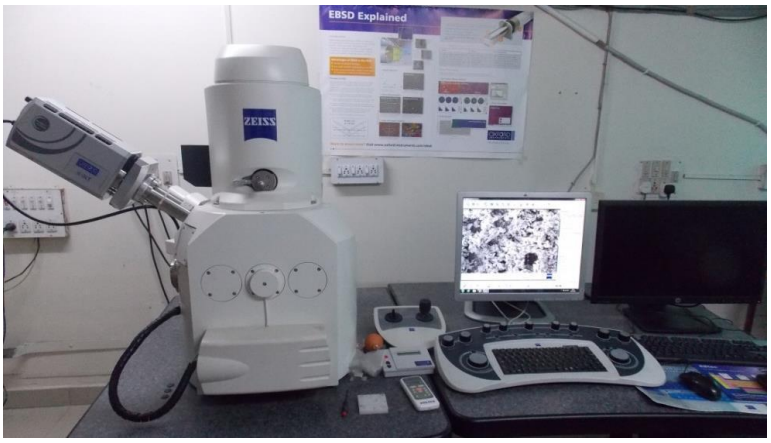

Fig. 4.6. Scanning electron microscope (ZEISS)

4.6 Mechanical Testing

In order to measure the ultimate tensile strength (UTS) of the FSPed samples, universal testing machine (TINIUS OLSEN, MODEL: H25KS) shown in Fig.4.7 was used. The tensile test also helped in finding out the yield strength (YS) and ductility of the material. The tensile specimen used for this purpose had the dimensions- gauge length of 10 mm, width of 2.5 mm and thickness of 2 mm.

The hardness values of the samples compacted at different compaction pressures before and after FSP were also measured. It was measured using the computerised Vicker's hardness Tester shown in Fig.4.8. During the test, a load of 1 kgf was applied and the dwell time used was 15 seconds for the indentation.

Fig. 4.7. Universal testing machine (TINIUS OLSEN,H25KS)

Fig. 4.8. Vickers Hardness Tester VM50 PC

4.7 XRD Analysis

X-ray diffraction (XRD; Cu K_α radiation) was utilised to identify the phases present in the Al-Cu specimen before and after FSP. The XRD scan was carried out within the angle range of 20 to 90 degrees using the machine shown in Fig.4.9. The scan rate used was. First of all, XRD of the 3 Al-Cu green compacts were done which showed the position of pure Al and pure Cu peaks. XRD of the FSPed samples was also carried out. The comparision of the XRD patterns before and after FSP for all the three compositions was done and the difference in the XRD patterns of the 3 FSPed samples was also studied. The phases formed in the specimen due to FSP was analysed.

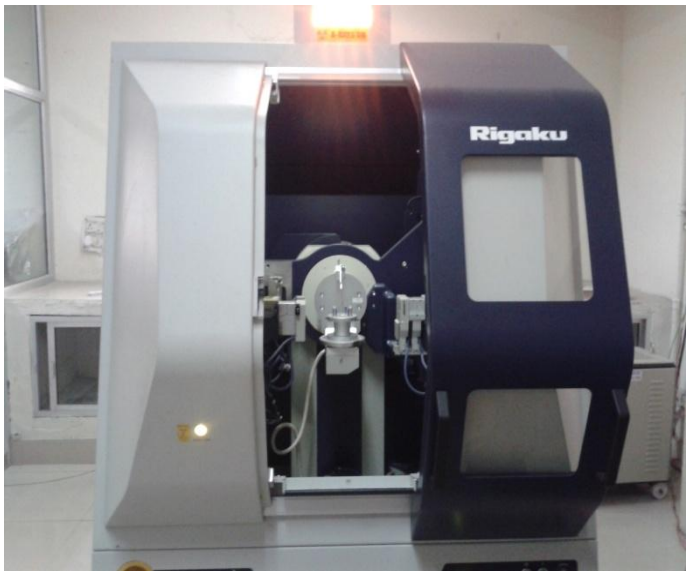

Fig. 4.9. X-Ray Diffraction (XRD) Machine (Rigaku)

5.1 Powder Characterization

Pure Aluminium and pure copper powder were both analysed under SEM to determine their morphology and particle size. The SEM images for the two powders are shown in Fig.5.1. It was found that both pure Al and pure Cu particles had an average size of 65 µm. The aluminium powder particles were mostly spherical in shape whereas the copper particles were distributed in the form of flakes.

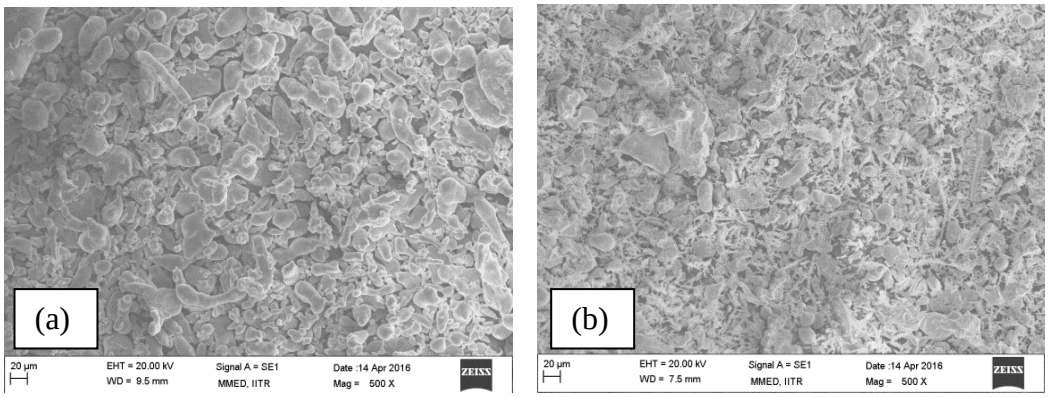

Fig. 5.1. SEM Images of (a) pure Al powder and (b) pure Cu powder

The course of work has been discussed under the following headings:

5.2 Effect of Compaction Pressure on FSPed Pure Aluminium Compact

The effect of the variation of compaction pressure on the feasibility of FSP on pure aluminium compact was studied. For this purpose, the samples were prepared at 7 different compaction pressures: 50 MPa, 100 MPa, 150 MPa, 200 MPa, 250 MPa, 320 MPa and 380 MPa. FSP was performed on all the green compacts using process parameters of 1525 rpm rotational speed and 1 mm/min traverse speed. It was observed that FSP was possible on all the green compacts. The effect of the compaction pressure on FSP of green compacts was studied under the sub headings as discussed below.

5.2.1 Microstructure Characterisation

The microstructure of the green compact, sintered specimen and the FSPed samples were observed under an optical microscope as well as scanning electron microscope (SEM). For obtaining the microstructure, a transverse section was cut from each of the FSPed samples.

One of such sample is shown in Fig.5.2. The microstructure of the green compact and FSPed region is shown in Fig.5.3.(a) and Fig.5.3.(b) respectively.In the microstructure of the green compact, the presence of particle boundaries were clearly observed as well as porosities inbetween them. During FSP as intense plastic deformation occurs at elevated temperatures, so an equiaxed fine grained structure was attained. The porosities were almost completely eliminated and a homogeneous microstructure was obtained after FSP.

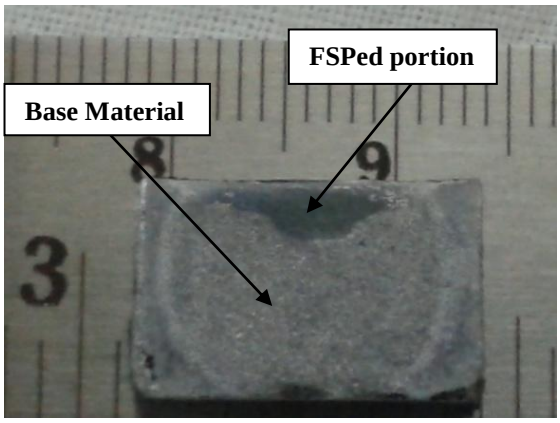

Fig. 5.2. Electropolished sample compacted at 200 MPa

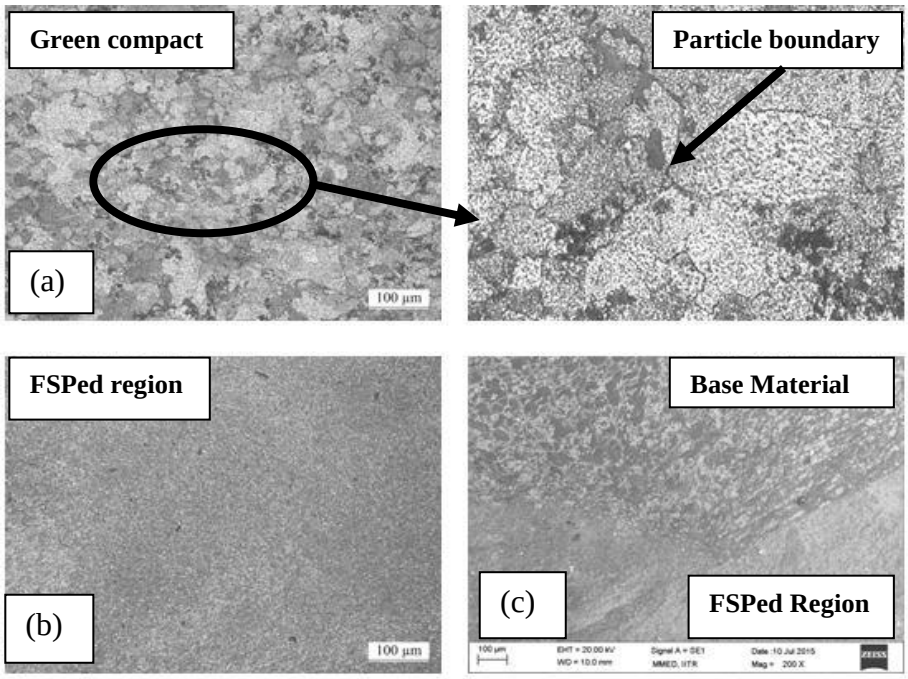

Fig. 5.3. (a) Microstructure of pure Al green compact (b) Microstructure after FSP and (c) Microstructure showing the different regions after FSP

Fig.5.3.(c) shows the partition region separating the FSPed zone from the base material region. As the grains were not clearly visible under Optical Microscope, so Electron Back

Scattered Diffraction (EBSD) was carried out to get an idea of the grain size after FSP and also about the grain boundary orientation. EBSD was performed on the FSPed region of the pure Al sample compacted at 200 MPa pressure. From the EBSD scan it was found out that the grains were equiaxed and the average grain size after FSP was around 3µm. Moreover sub grains were also seen to be present. Fig.5.4.(a) and Fig.5.4.(b) shows the EBSD scan of FSPed region of 200 MPa compacted sample and the number fraction vs misorientation angle plot respectively. The grains with different orientation angles were denoted by different colours.The grain size was checked on FSPed samples compacted at two other different compaction pressures as well. It was seen that the average grain size obtained in all the cases were near about the same i.e around 3µm. Thus the variation in compaction pressure did not have any significant effect on the microstructure of the FSPed samples. Moreover it was also seen that after FSP larger fraction of grain boundaries were low angle grain boundaries. This indicated the presence of sub-grains which is a result of incomplete recrystallization.

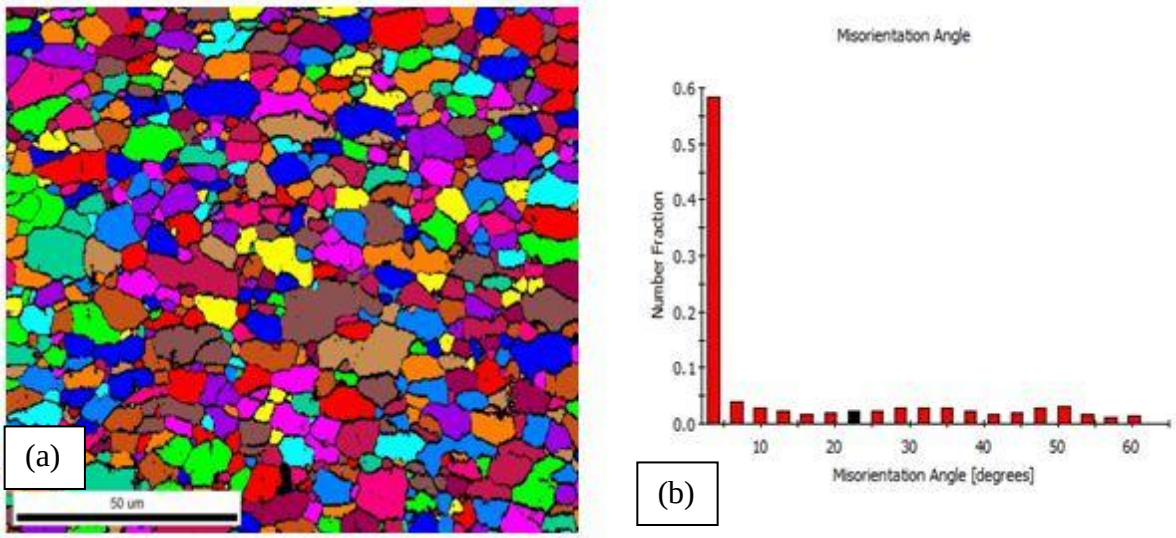

Fig. 5.4.(a) EBSD Scan of FSPed region of 200 MPa sample and (b) Number fraction vs Misorientation angle plot of FSPed region

5.2.2 Density and Porosity

During compaction, the material gets densified mainly in two stages. Firstly the particles get re-arranged and contact points get established between the powder particles. As compression continues, increasing forces act on these contact points resulting in cold pressure welding. This increases the density to some extent. In the next stage, the stresses between the powder particle contact points causes material deformation. Contact areas are

increased, interlocking and plastic flow of particles occurs, volume decreases and density continues to rise. Material movement is opposed by friction and work hardening of metal powder results in increase in density. During FSP, intense plastic deformation occurs at elevated temperatures. As high amount of heat gets generated, so the material softens and starts to flow from the front to the back of the pin. Thus, an equiaxed and fine grained microstructure is obtained after FSP. The porosities get almost totally eliminated. The density of the green compacts before and after FSP was measured using the Archimedes principle set up. The relative density values have been shown in Table 1 and the comparision between green relative density and FSPed relative density is shown in the form of bar diagram in Fig.5.5..It is to be noted that the theoretical density of pure Al is 2.7 g/cm^3.

It was found that the densities of the green compacts increased uniformly with the increase in the compaction pressure till 200 MPa compaction pressure after which there is a slight fall in density. This may be attributed to the spring back effect occurring at higher compaction pressures. Maximum relative density of 95.33% was obtained in case of the 200 MPa sample. After FSP, the values of densities of all the compacts reached almost equivalent to the value of the theoretical density. Thus after FSP, there was a significant reduction in the porosity level.

Table 1. Density Measurement of Green and FSPed samples

S. No.	Compaction Pressures (MPa)	Green Density (g/cm^3)	Green Relative Density (%)	Porosity (%)	FSPed Density (g/cm^3)	FSPed Relative Density (%)	Porosity (%)
1	50	2.36	87.40	12.60	2.67	99.20	0.80
2	100	2.43	89.88	10.12	2.68	99.25	0.75
3	150	2.52	93.36	6.64	2.69	99.48	0.52
4	200	2.57	95.33	4.67	2.70	100	0
5	250	2.54	94.02	5.98	2.70	100	0
6	320	2.56	94.74	5.26	2.70	100	0
7	380	2.46	91.19	8.81	2.63	97.52	2.48

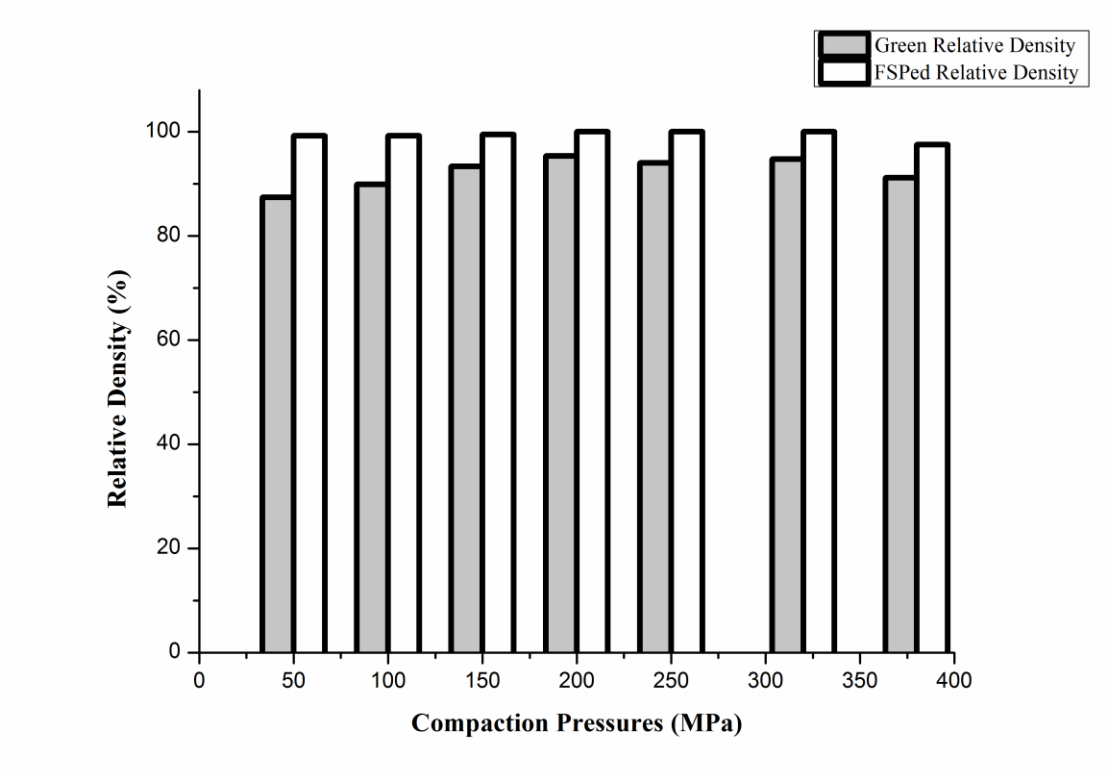

Fig. 5.5. Bar diagram comparing the relative densities of compacts before and after FSP

5.2.3 Mechanical Properties

5.2.3.1 Hardness

The hardness values of the samples were measured using the computerized Vickers Hardness Tester. The values of hardness of the compacts before and after FSP were compared. It was found with the increase in the compaction pressure, the hardness of the green compacts also increased but the amount of increase was not that significant. However the hardness of the FSPed portion was considerably high in comparision to that of the base material region. This is because after FSP, almost all the porosities get eliminated and a fine grained microstructure is obtained. The increase in hardness from base material region to FSPed region was found to be maximum in case of 200 MPa sample. The hardness values increased by over 140%.The hardness values of the base material and that of FSPed region for all seven compacts is shown in Table 2 and the comparision between base and FSPed hardness is shown in Fig.5.6.

Table 2. Hardness Measurement of Base material and FSPed region

S. No.	Compaction Pressures (MPa)	Hardness of Base Material (HV)	Hardness of FSPed portion (HV)
1	50	29.2± 3	51.6± 2
2	100	32.2± 5	53.9± 3
3	150	33.1± 3	54.2± 2
4	200	33.4± 2	54.5± 2
5	250	35.3± 4	57.1± 3
6	320	36.7± 5	59.7± 3
7	380	38.3± 4	60.2± 2

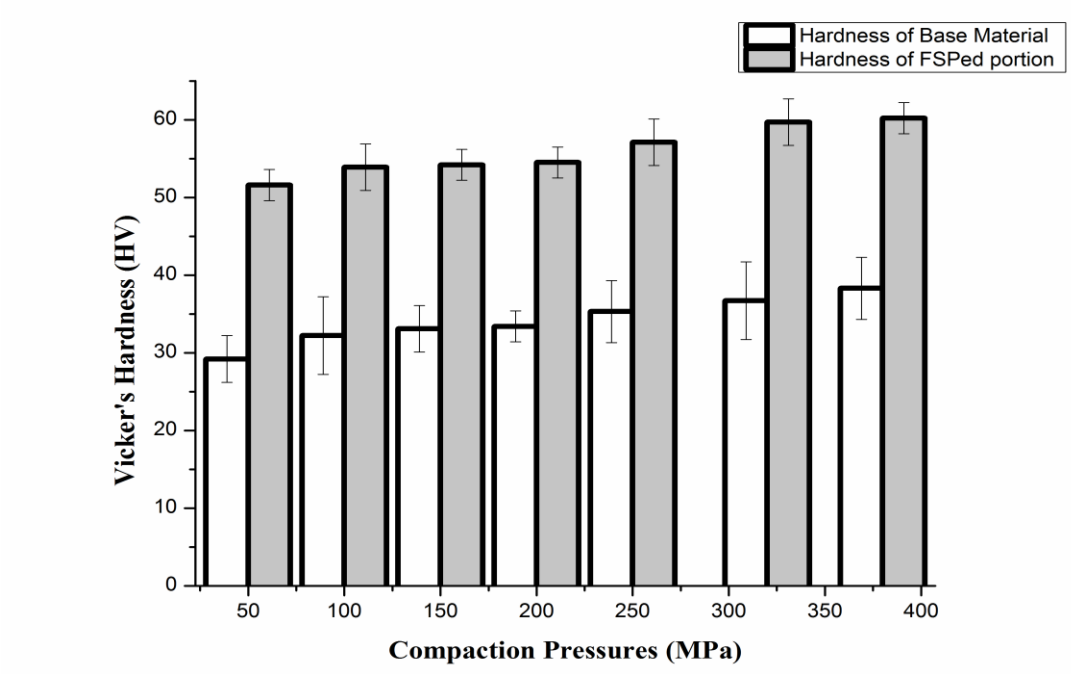

Fig. 5.6. Bar diagram comparing the average hardness values of all 7 samples before and after FSP

5.2.3.2 Tensile Properties

The Universal Testing Machine was used to measure the Ultimate Tensile Strength, Yield Strength and Ductility of the green compacts after FSP. The specimen used for the test is shown in Fig.5.7.

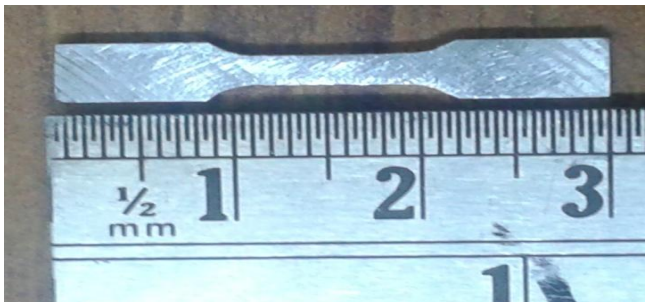

Fig. 5.7. Snapshot of the Tensile Specimen

From the results of the test, it was observed that the FSPed samples which were compacted at low compaction pressures showed both greater tensile strength as well as elongation. Out of all the FSPed samples, the sample compacted at 200 MPa showed the best results after FSP i.e UTS of 153.4 MPa and elongation of 37.8%. This is because at this particular pressure the material movement was occurring as desired. At too high pressures, due to inadequate material movement, the properties obtained were comparatively inferior. The values of UTS and maximum elongation for all 7 FSPed samples is shown in Table 3 below: Fig.5.8 shows the stress vs strain curves for all 7 FSPed samples whereas Fig.5.9.(a) and Fig.5.9.(b) shows the comparision between UTS and elongation values respectively for the samples in the form of bar diagram.

Table 3. Measurement of UTS and Maximum Elongation of 7 samples

S.No.	Compaction Pressures (MPa)	Ultimate Tensile Strength (MPa)	Maximum Elongation (%)
1	50	129.09	28.4
2	100	100.14	25.8
3	150	146.63	30
4	200	153.4	37.8
5	250	93.5	14.7
6	320	105.03	20.4
7	380	110	18.2

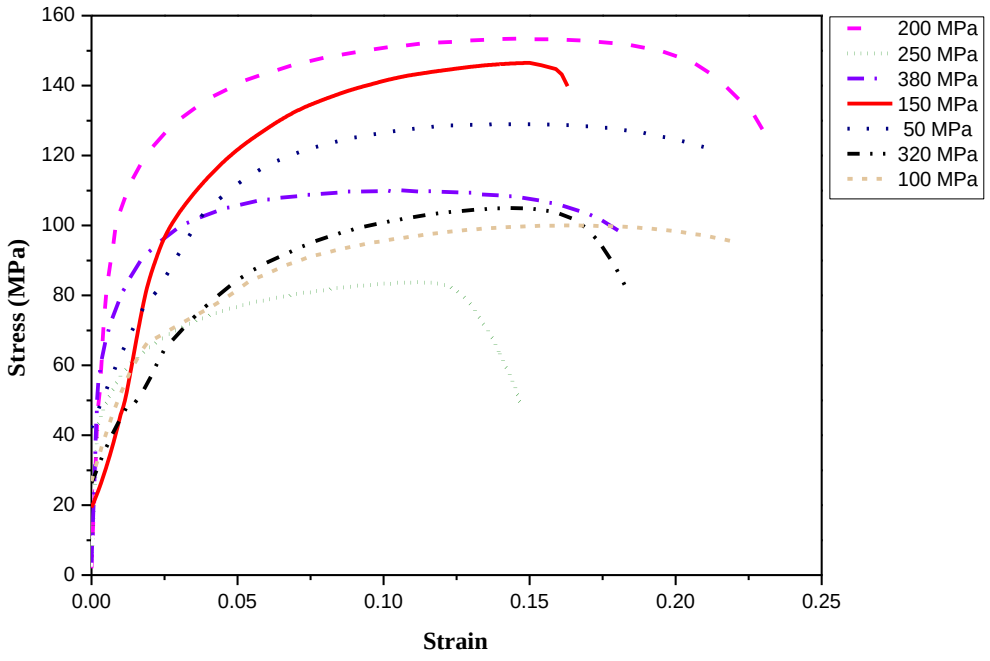

Fig. 5.8. Stress vs Strain Curves for FSPed samples compacted at 7 different compaction pressures

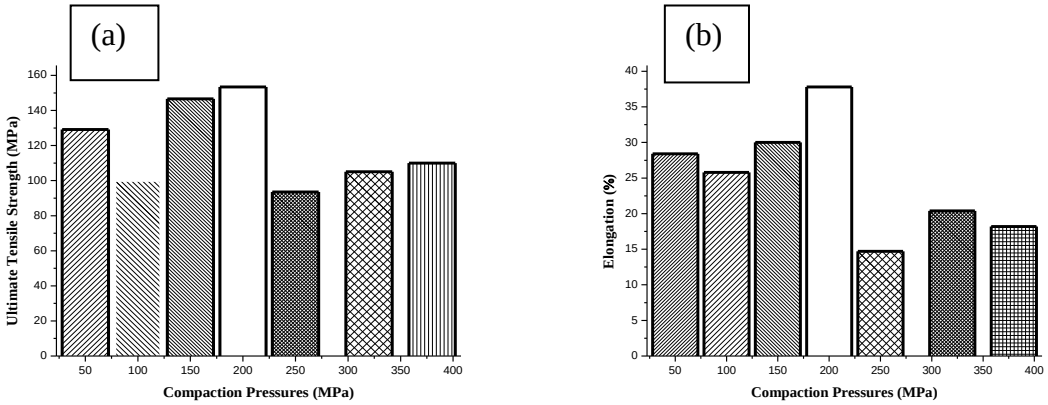

Fig. 5.9. Bar diagram comparing the (a) UTS values and (b) Maximum Elongation values of FSPed samples compacted at 7 different compaction pressures

5.2.4 Fractrography

Fractography was performed on all the 7 samples processed under conditions of 1525 rpm and 1 mm/min. The fractured surfaces were viewed under SEM to support the mechanical properties. The fractured surfaces of the FSPed samples compacted at 200 MPa, 250 MPa, 100 MPa and 380 MPa are shown in Fig.5.10.(a), Fig.5.10.(b), Fig.5.10.(c) and Fig.5.10.(d) respectively. It is clearly seen that there is dimple morphology in all the cases thereby supporting ductile fracture. But there is a marked difference in the morphology of the dimples in the four cases. In case of 200 MPa fractured surface i.e the sample which showed maximum ductility as well as strength, the dimples are of smaller size and uniformly distributed but in case of 250 MPa i.e the sample with least ductility, the size of the dimples are larger and very unevenly distributed. Thus we can conclude that smaller dimples can be related to more resistance to failure in comparision to larger dimples.

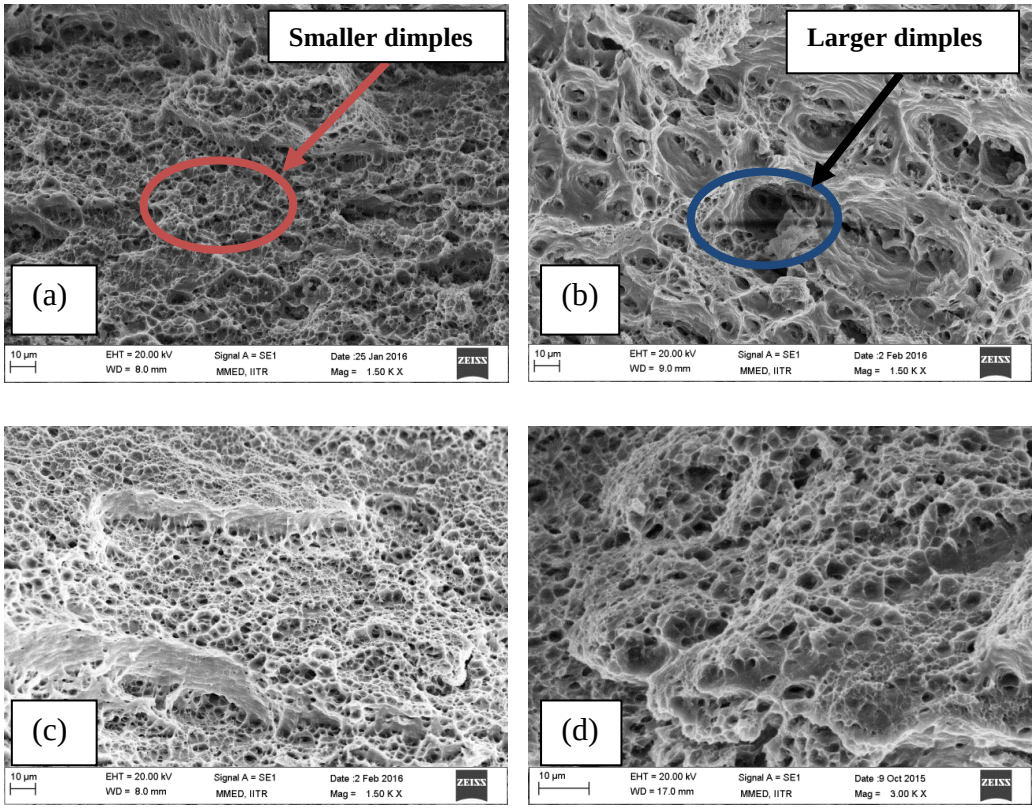

Fig. 5.10. Fractured surface of sample processed under conditions of 1525 rpm and 1 mm/min (a) compacted at 200 MPa (b) compacted at 250 MPa (c) compacted at 100 MPa and (d) compacted at 380 MPa

5.3 Comparision between Green FSPed and Sintered FSPed samples compacted at 200 MPa

From the earlier study, it was found that the FSPed sample compacted at 200 MPa showed the best results so it was considered for further study. The next objective was to perform a comparative study between green FSPed and sintered FSPed samples compacted at 200 MPa. For this purpose, the 200 MPa compacted sample was sintered at 610˚C for a holding time of 1 hour in a tube furnace in presence of atmosphere of N_2 gas. After sintering, FSP was performed using the same process parameters of 1525 rpm and 1mm/min. As sintering of pure Al is very difficult due to formation of surface oxides, so another sample was prepared in which 0.5% Mg was added to pure Al. The Al and Mg powders were mixed thoroughly in desired proportions in a mortar and pestle for around 10 minutes. Magnesium forms a spinel compound $MgAlO_4$ during sintering and hence helps in proper sintering of pure Al compact. The sintered sample was then FSPed using the same process parameters. The comparative study between green FSPed and sintered FSPed samples was done under the following sub headings:

5.3.1 Microstructure Characterization

The microstructure of the green and sintered specimen compacted at 200 MPa were observed. In case of the green compacts, the presence of particle boundaries was clearly visible with porosities in between them as seen in Fig.5.11.(a). After sintering, as necking occurs between the powder particles, the porosities get reduced to a great extent as shown in Fig.5.11.(b).The microstructure of the FSPed sample is shown in Fig.5.11.(c). There occurs intense plastic deformation during FSP which resulted in equiaxed and fine grained microstructure.

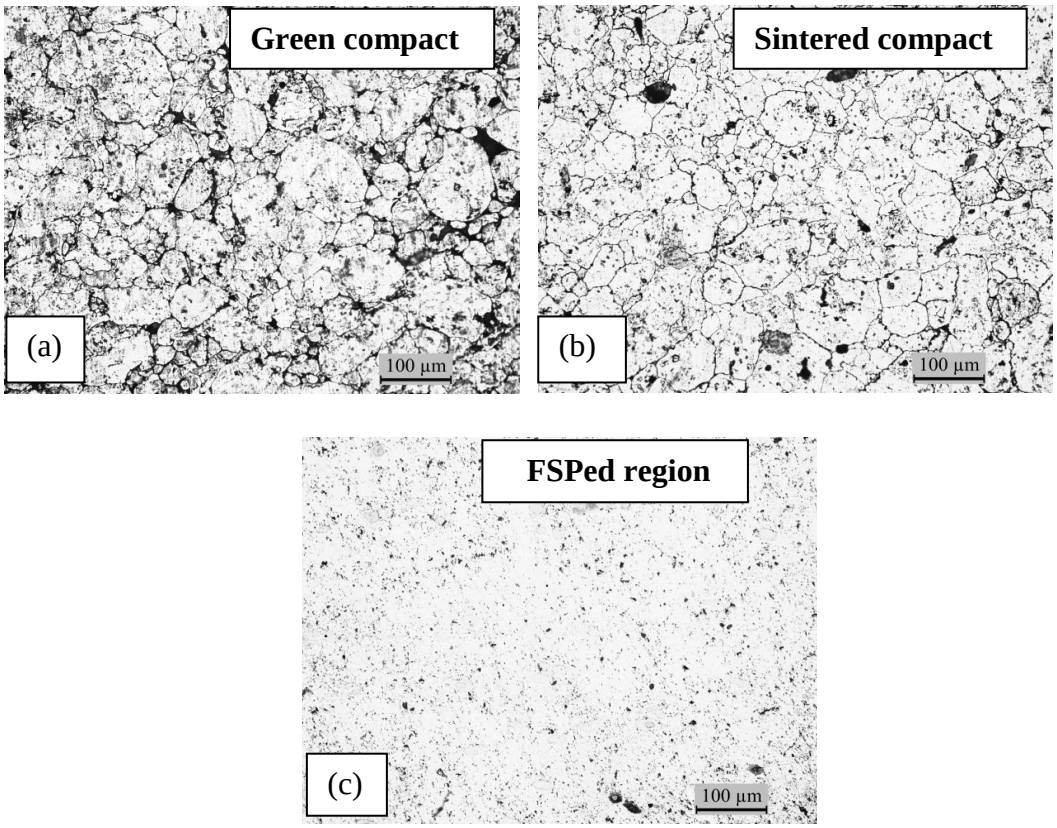

Fig. 5.11. Microstructure of (a) Green compact and (b) Sintered sample both compacted at 200 MPa and (c) Microstructure of the sample after FSP

The microstructure of the green compact and that of the sintered specimen was also observed under SEM. Fig.5.12.(a) and Fig.5.12.(b) shows the SEM image of green compact and sintered specimen respectively.It is evident that after sintering the particle boundaries and porosities get reduced to considerable extent.

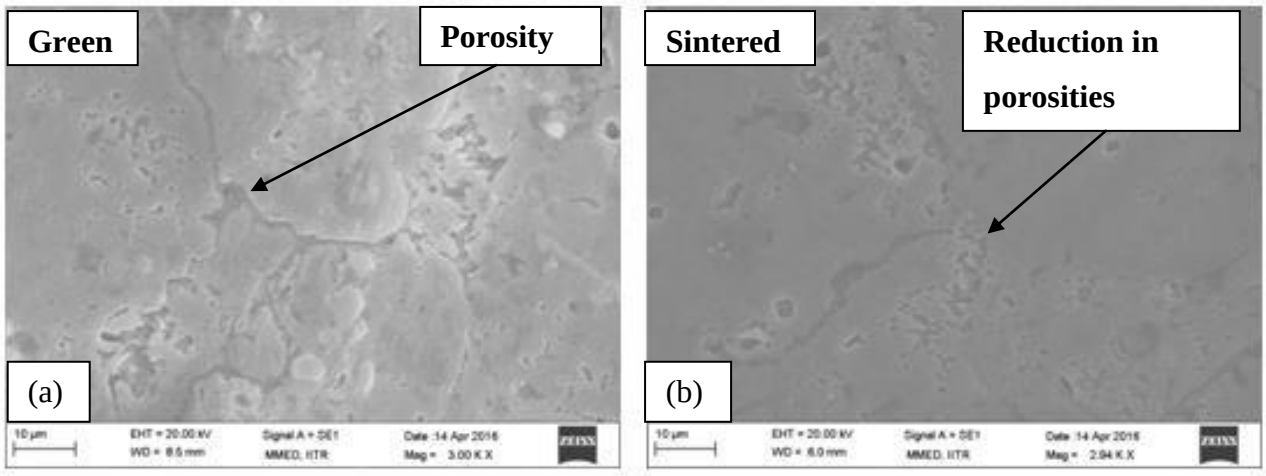

Fig. 5.12. SEM images of (a) Green and (b) Sintered sample compacted at 200 MPa

5.3.2 Density and Porosity

The calculation of density and reduction in porosity after FSP was carried out. The density was measured using the Archimedes principle setup. It was found that there was an increase in density of the compacted sample after sintering as compared to the green compact. After FSP as all the porosities got almost eliminated so the density values approached the theoretical density value. So the density of the samples after FSP for both green and sintered condition were almost the same.Table 4 shows the porosity percentages for all 4 samples before and after FSP. Fig.5.13 shows the comparision between green/sintered hardness and FSPed hardness for all 4 samples.

Table 4. Density measurement of 200 MPa Green and Sintered Samples before and after FSP

S. No.	Composition	Green/ Sintered Density (g/cm^3)	Green/ Sintered Relative Density (%)	Porosity (%)	FSPed Density (g/cm^3)	FSPed Relative Density (%)	Porosity (%)
1	Pure Al (green)	2.57	95.33	4.67	2.69	99.59	0.41
2	Pure Al (sintered)	2.59	96.11	3.89	2.68	99.51	0.49
3	Al-0.5wt%Mg (green)	2.56	95.37	4.63	2.68	100	0
4	Al-0.5wt%Mg (sintered)	2.60	96.76	3.24	2.67	99.36	0.64

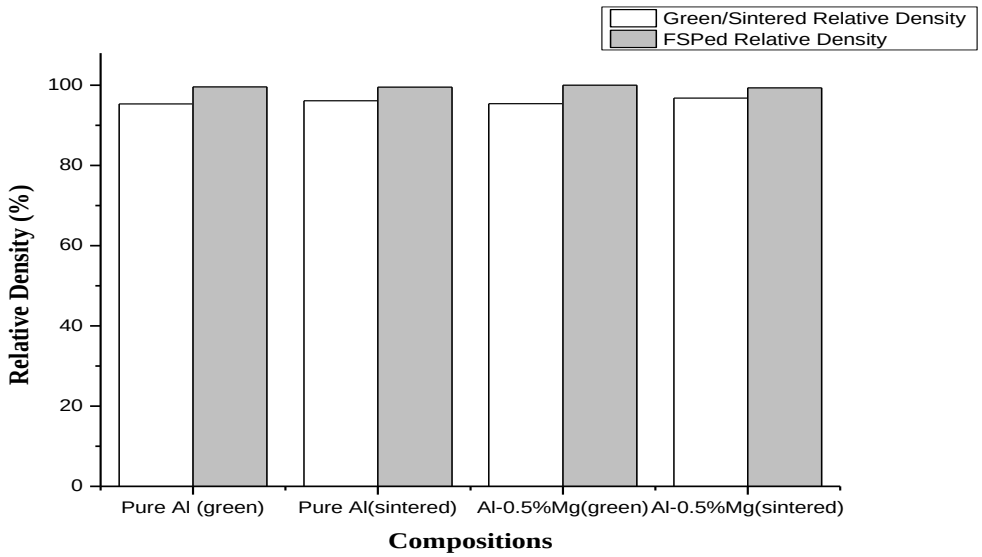

Fig. 5.13. Bar diagram indicating the relative densities of samples before and after FSP

5.3.3 Mechanical Properties

5.3.3.1 Hardness

The values of hardness for both green and sintered samples before and after FSP was measured using the Computerized Vicker's Hardness Tester.Table 5 shows the hardness values for all the 4 samples before and after FSP. It was observed that on addition of Mg to pure Al, the values of hardness of base material increased a bit but the amount of increase was not that significant. Moreover the sintered samples showed greater hardness values as compared to the green compacts. After FSP, there was considerable increase in the hardness in comparision to the green or sintered hardness. This is mainly because of the reduction in porosity and also the grain boundary strengthening which takes place during FSP on pure Al. A bar diagram showing the comparision between green/sintered hardness and FSPed hardness is shown in Fig.5.14.

Table 5. Hardness Measurement of Green, Sintered and FSPed 200 MPa compacted sample

S. No.	Compositions	Hardness of Base Material (HV)	Hardness of FSPed portion (HV)
1	Pure Al (green)	33.4± 2	54.5± 2
2	Pure Al (sintered)	35.4± 3	55.4± 4
3	Al-0.5wt% Mg(green)	35.6± 2	58.7± 3
4	Al-0.5wt% Mg(sintered)	36.2± 4	58.2± 2

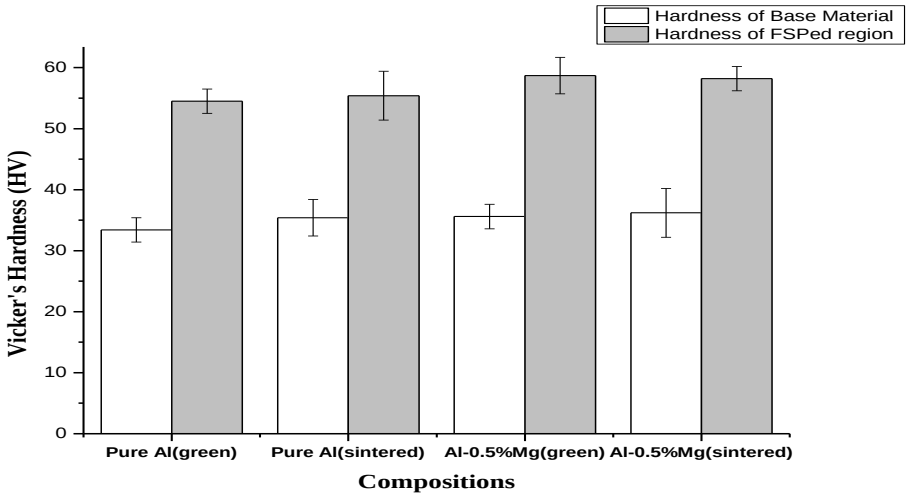

Fig. 5.14. Bar diagram comparing base and FSPed hardness of the 4 samples

5.3.3.2 Tensile Properties

The tensile properties and ductility values were determined using the universal testing machine. Table 6 shows the ultimate tensile strength (UTS) and maximum elongation values for the specimen under the 4 different conditions. It was observed that on addition of Mg to pure Al although the tensile strength increased a bit but the value of ductility got reduced significantly.

The maximum strength obtained was in case of Al-0.5wt%Mg (green+FSPed) which was around 165 MPa and the maximum ductility was around 38% in case of pure Al (green+FSPed). Thus it was seen that the sintered plus FSPed samples showed both lesser strength as well as ductility in both the cases. The reason for such behaviour cannot be ascertained certainly. It requires a more detailed study.Fig.5.15 shows the stress vs strain curves for all 4 FSPed samples. The comaparision between the UTS values and the maximum elongation values for all the 4 samples has been shown in the form of bar diagrams in Fig.5.16.(a) and Fig. 5.16.(b) respectively.

Table 6. Measurement of UTS and Maximum Elongation

S. No.	Compositions	Ultimate Tensile Strength (MPa)	Maximum Elongation (%)
1	Pure Al (green+FSPed)	153.4	37.8
2	Pure Al (sintered+FSPed)	105.53	29
3	Al-0.5wt%Mg(green+FSPed)	165.1	18.4
4	Al-0.5wt%Mg(sintered+FSPed)	108.5	8.27

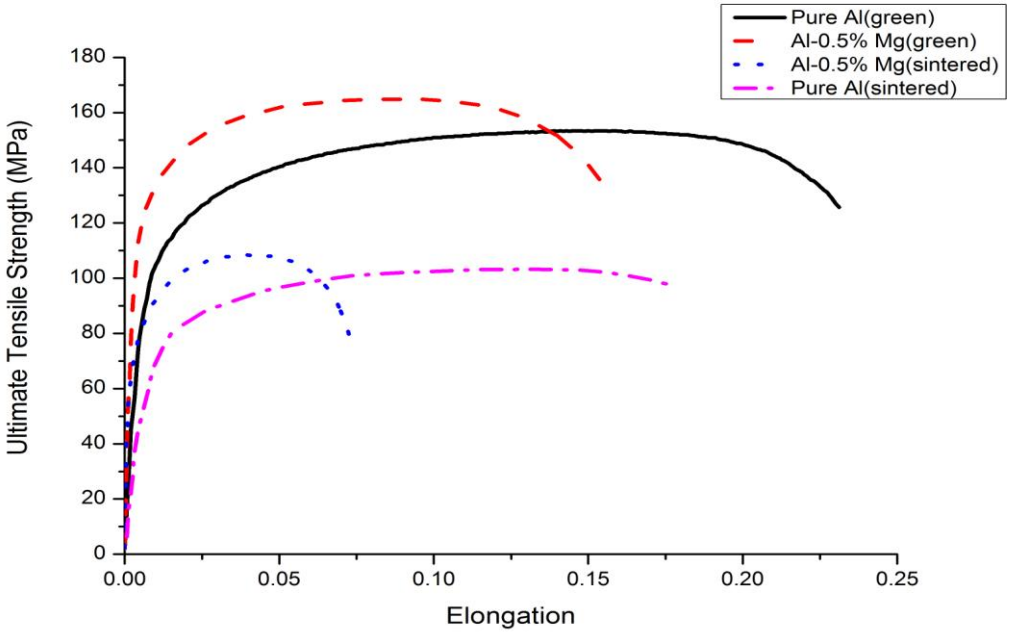

Fig. 5.15. Stress vs strain curves for pure Al and Al-0.5%Mg green and sintered FSPed samples

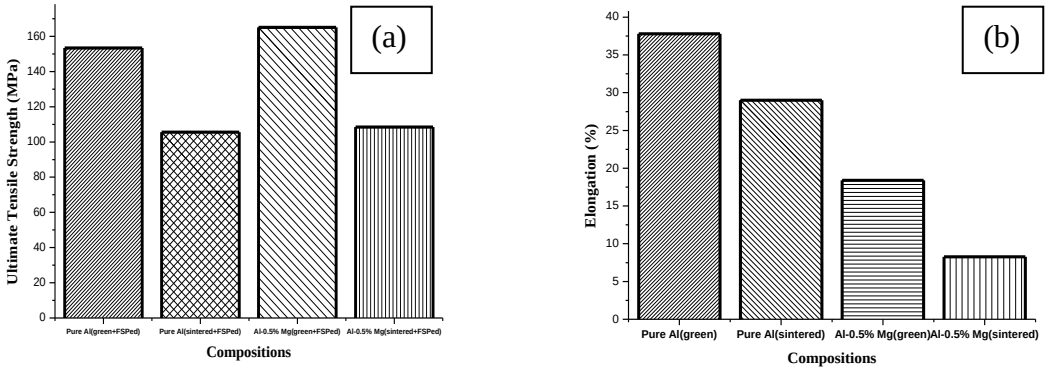

Fig. 5.16. Bar diagram comparing the values of (a) UTS and (b) maximum elongation for the 4 FSPed samples

5.3.4 Fractography

The fractured surface of the green FSPed as well as sintered FSPed samples compacted at 200 MPa were observed under SEM in order to ascertain the cause of failure. As evident from Fig.5.17.(a) and Fig.5.17.(b), dimples were observed in both the cases indicating ductile mode of fracture although there was difference in the size and morphology of the dimples.

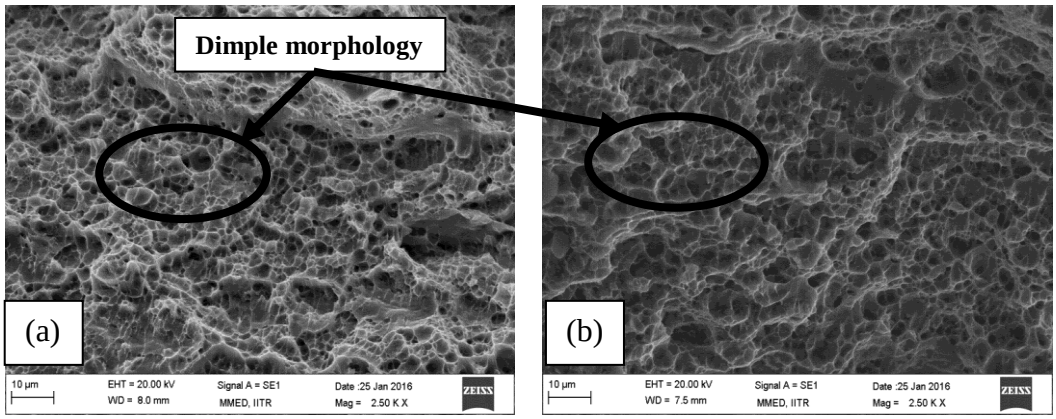

Fig. 5.17. Fractured surfaces of (a) green FSPed and (b) sintered FSPed samples both compacted at 200 MPa and processed under conditions of 1525 rpm and 1 mm/min

5.4 Effect of addition of Copper to Aluminum matrix

Next the effect of addition of copper particles into the aluminium matrix was studied. For this purpose three compositions were decided: Al-1wt%Cu, Al-5wt%Cu and Al-10wt%Cu. The powders were properly mixed in a ball milling machine. The mixing was done for 6 hrs at a speed of 100 rpm. Then the green compacts were compacted in the Cold Isostatic Press (CIP) machine using the same compaction pressure of 200 MPa. Finally, FSP was performed on the green compacts using the process parameter of 1525 rpm and 1 mm/min. The effect of the variation in copper content was studied under the following heads.

5.4.1 Microstructure Characterization

The microstructure of the Al-Cu samples were observed under both Optical as well as Scanning Electron Microscope. The copper particles were seen to be uniformly distributed in the aluminium matrix in case of the green compact as shown in Fig.5.18.(a). In case of the FSPed region, the particles could not be clearly distinguished under Optical Microscope as evident from Fig.5.18.(b). So it was viewed under Scanning Electron Microscope which showed the presence of some light coloured particles in the black matrix

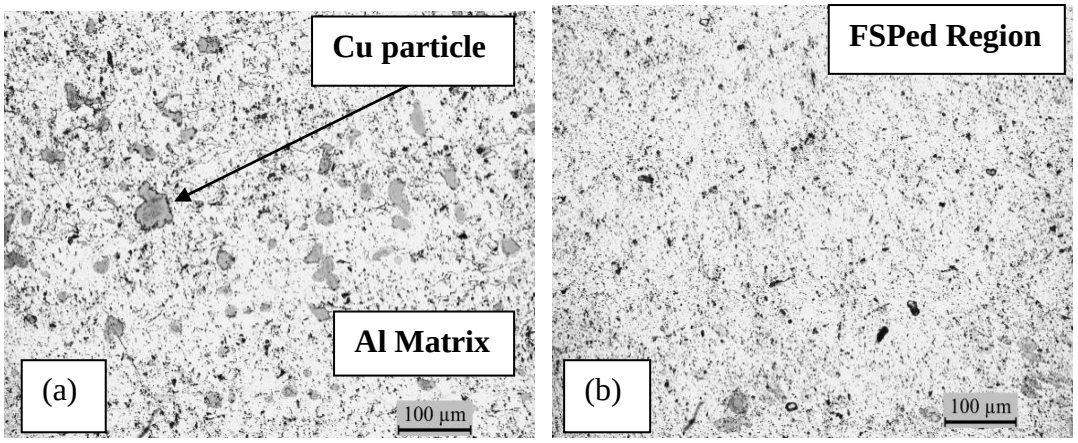

Fig. 5.18. Microstructure of (a) Al-10wt%Cu green compact and (b) Al-10wt%Cu FSPed sample

Then EDS was applied to identify the composition of those particles. Fig.5.19 shows the SEM images of the FSPed region of Al-10wt%Cu sample. In Fig.5.19.(a) the spectrum selected was the light coloured portion and the EDS results suggested that it was the Cu rich portion and in Fig.5.19.(b) the spectrum selected was the black matrix and the results suggested that it was the Al rich region. Thus after FSP, copper particles entered into the aluminium matrix and vice versa also took place. Fig. 5.20 shows the EDS mapping of Al-

10wt%Cu powder mixture. From the mapping results, it could be concluded that the powders were mixed homogenously.

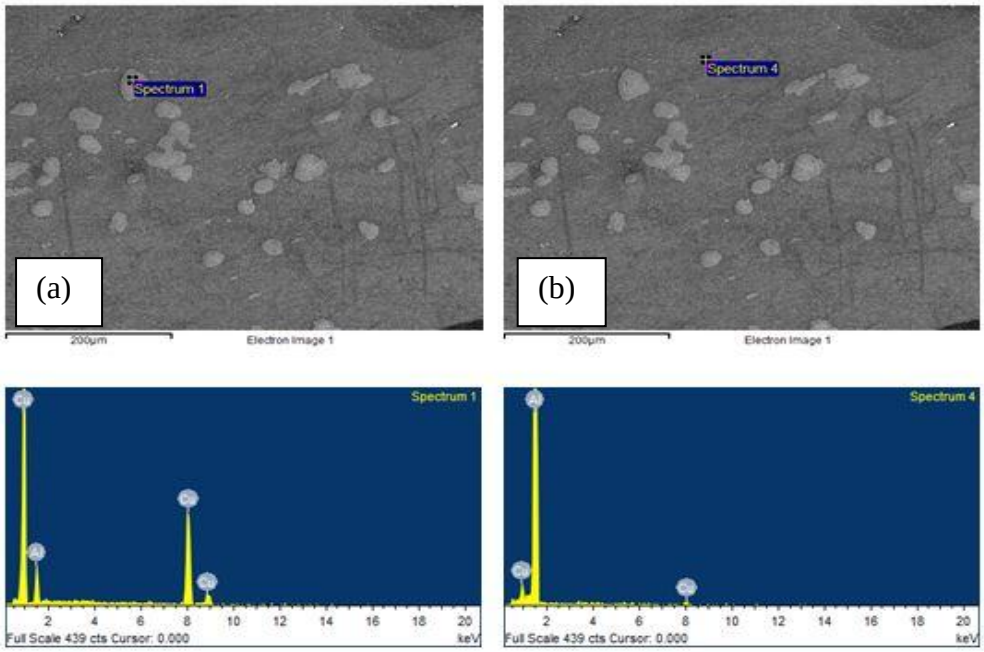

Fig. 5.19. EDS Analysis of FSPed region of Al-10wt% Cu sample

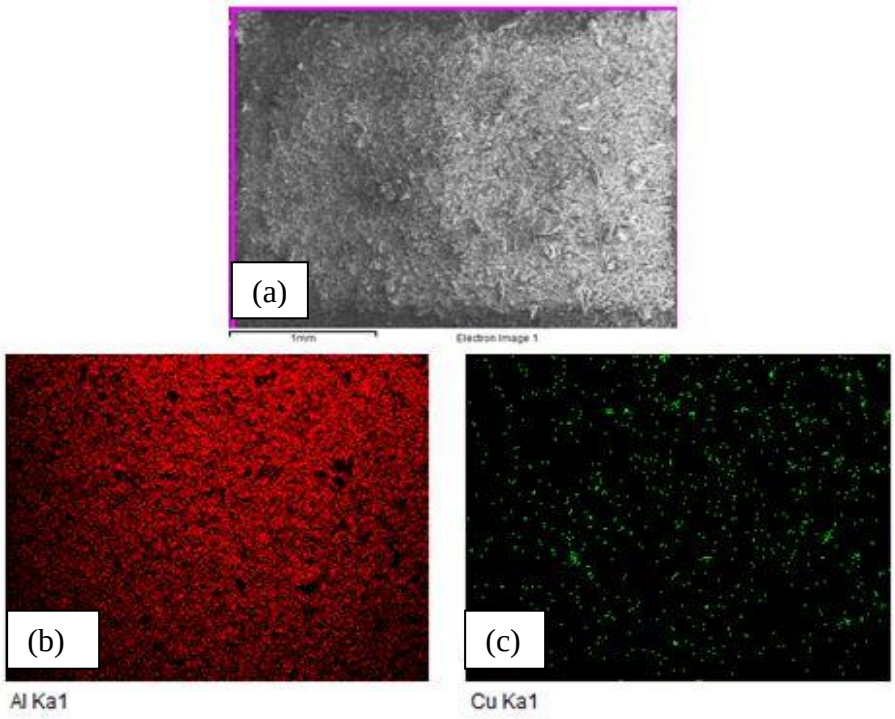

Fig. 5.20. EDS Mapping images showing (a) the area of observation (b) distribution of Al and (c) distribution of Cu in Al-10wt%Cu powder mixture

Fig.5.21 shows the EDS analysis of the FSPed region of Al-1wt%Cu sample. In Fig.5.22 the EDS analysis of FSPed region of Al-5wt%Cu is shown.It is evident from the results that as the spectrum selected is moved away from the light coloured region, the percentage of copper also went on decreasing. From this, it could be concluded that the light coloured regions were rich in copper.

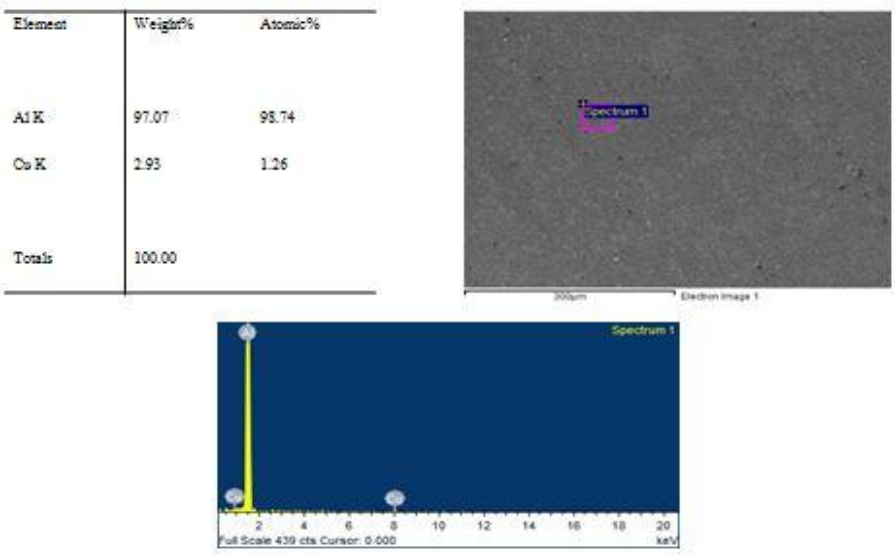

Fig. 5.21. EDS Analysis of Al-1wt%Cu sample

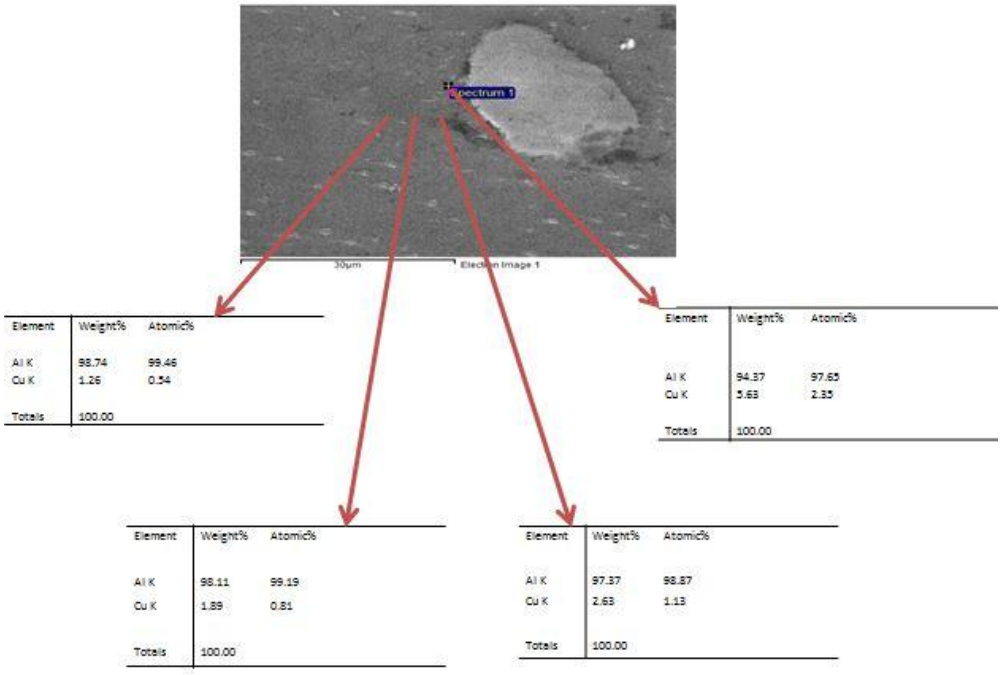

Fig. 5.22. EDS Analysis of Al-5wt%Cu showing the variation of Cu content as the region of selection is moved away from the light coloured region

5.4.2 Density and Porosity

The density values of the three Al-Cu samples were calculated and compared with the pure Al sample as shown in Table 8 and Fig.5.23. It was seen that as earlier a very high density of around 96% was obtained in case of green compacts and after FSP, the porosities were almost totally eliminated giving a density value almost equal to theoretical density. The theoretical density values for different compositions of Cu in Al-Cu composite are shown in Table 7 below:

Table 7. Theoretical density values for various compositions

S.No.	Composition	Theoretical Density (g/cm^3)
1	Pure Al	2.70
2	Al-1wt%Cu	2.72
3	Al-5wt%Cu	2.80
4	Al-10wt%Cu	2.9

Table 8. Density measurement of Al-Cu samples and comparision with pure Al

S. No.	Composition	Green density (g/cm^3)	Green Relative Density (%)	Porosity (%)	FSPed Density (g/cm^3)	FSPed Relative Density (%)	Porosity (%)
1	Pure Al	2.57	95.33	4.67	2.69	99.59	0.41
2	Al-1wt%Cu	2.64	97.19	2.81	2.70	99.70	0.30
3	Al-5wt%Cu	2.69	96.12	3.88	2.77	99	1
4	Al-10wt%Cu	2.78	95.80	4.2	2.90	100	0

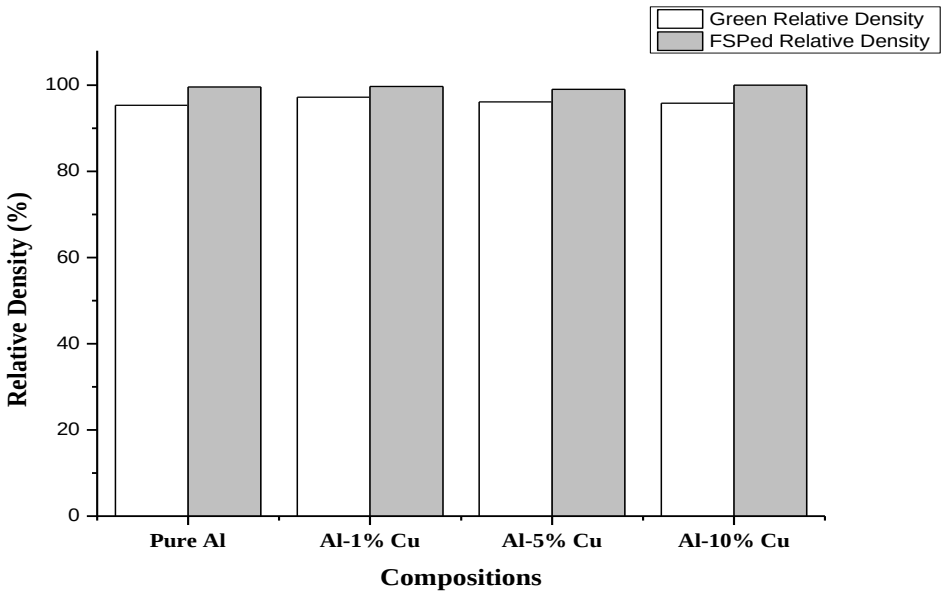

Fig. 5.23. Bar diagram comparing the relative density values before and after FSP

5.4.3 XRD Analysis

X-ray diffraction (XRD) was utilized in order to find out the phases formed in the specimen. XRD was performed for all the three compositions i.e Al-1wt%Cu, Al-5wt%Cu and Al-10wt%Cu in case of both green as well as FSPed samples. In case of the green compacts, the XRD results showed peaks of pure Al and pure Cu. But it was seen that after FSP, the pure Cu peaks got vanished although the pure Al peaks were still present. In addition to pure Al, some peaks of metal oxides like CuO etc and some peaks of intermetallic compounds like Al_2Cu etc were also present. The formation of these intermetallic compounds and metal oxides led to greater strength after FSP in addition to contribution due to grain refinement.Fig.5.24, Fig.5.25 and Fig.5.26 compares the XRD patterns of Al-1wt%Cu, Al-5wt%Cu and Al-10wt%Cu before and after FSP. Fig.5.27 shows a comparision between the XRD patterns of the FSPed samples for all three compositions.

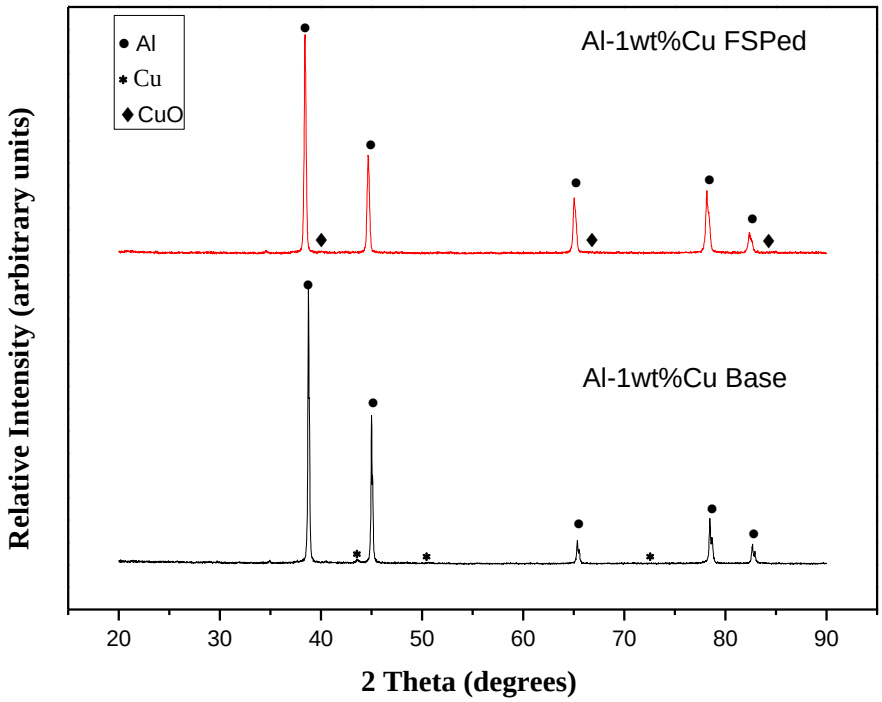

Fig. 5.24. XRD pattern of Al-1wt%Cu sample before and after FSP

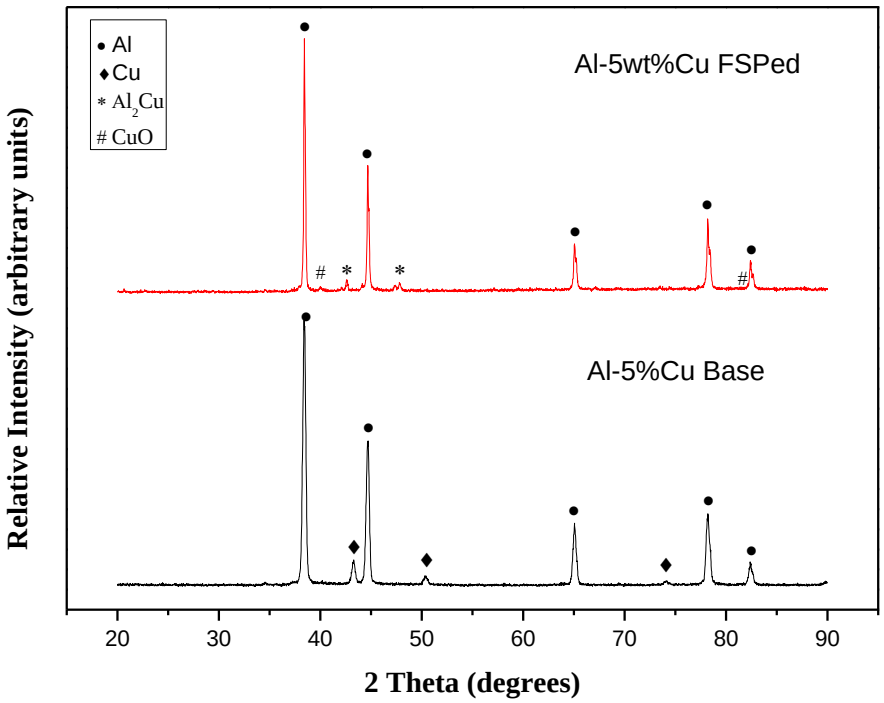

Fig. 5.25. XRD pattern of Al-5wt%Cu sample before and after FSP

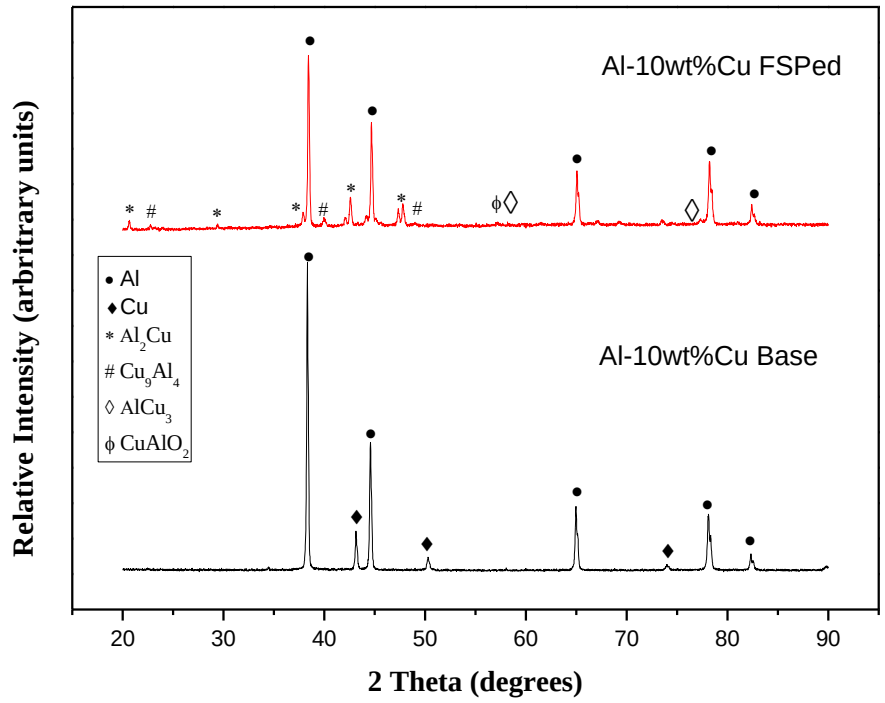

Fig. 5.26. XRD pattern of Al-10wt%Cu sample before and after FSP

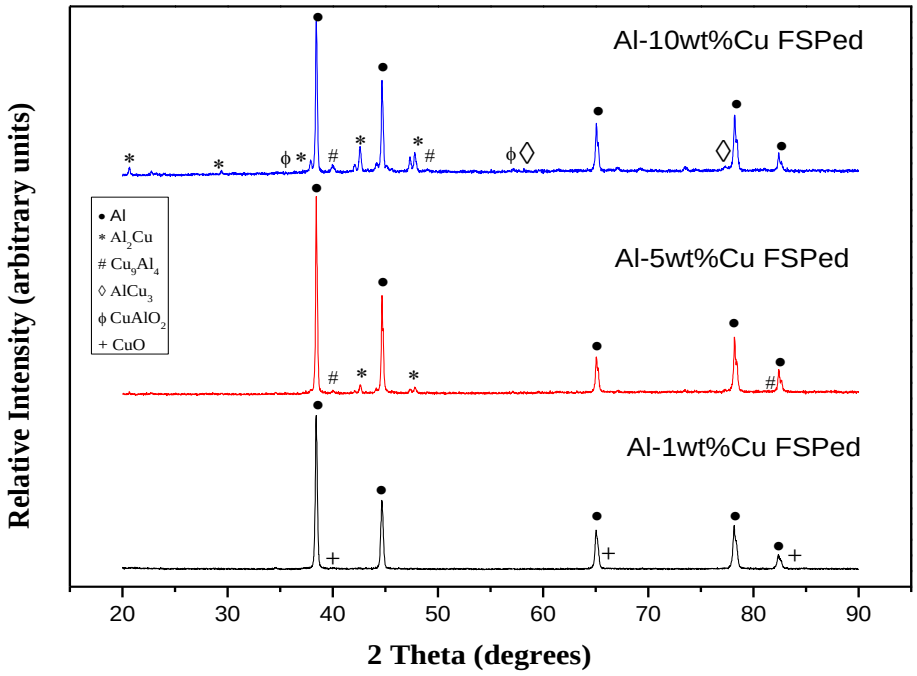

Fig. 5.27. XRD pattern of Al-Cu samples after FSP

5.4.4 Mechanical Properties

5.4.4.1 Hardness

The hardness values of all the 3 Al-Cu samples both before and after performing FSP were measured using the Vickers Hardness Tester. The values were compared with that of pure Al sample as shown in Table 9. It was seen that the base hardness values increased uniformly with increase in Cu content although the amount of increase is not that significant. But it is also to be noted that the hardness of the material increased considerably after FSP in comparision to the base material. Out of the three compositions it is seen that in case of Al-5wt%Cu and Al-10wt%Cu, the hardness values after FSP has increased relatively more in comparision to pure Al or Al-1wt%Cu. The main reason behind this is that as the Cu content is increased, in addition to grain boundary strengthening, the solid solution strengthening also comes into play. This results in increased hardness.

Table 9. Hardness measurement of Al-Cu samples before and after FSP

S.No.	Composition	Base Hardness (HV)	FSPed Region Hardness (HV)
1	Pure Al	33.4±2	54.5±2
2	Al-1wt% Cu	34.3±3	56.3±4
3	Al-5wt% Cu	36.5±4	57.5±3
4	Al-10wt% Cu	38.2±3	59.2±2

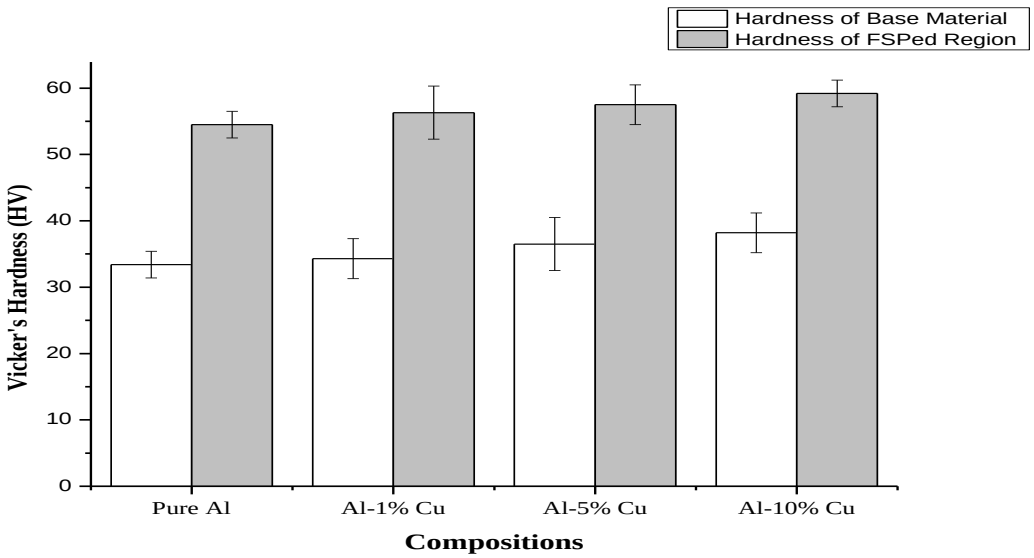

Fig. 5.28. Bar diagram showing hardness values of Al-Cu samples along with pure Al before and after FSP

5.4.4.2 Tensile Properties

The Ultimate Tensile Strength (UTS) and the maximum elongation of the samples after addition of Cu and performing FSP was calculated and the values are shown in Table 10. The FSP process parameter used were: rotational speed of 1525 rpm and traverse speed of 1 mm/min. It was observed that the strength increased uniformly with the increase in Cu content upto a certain point after which it decreased. The ductility value showed a gradual decrease with increasing Cu content. The strength of Al-1wt%Cu and Al-5wt% Cu after FSP was found to be more with respect pure Al FSPed sample. But the strength got decreased in case of Al-10wt%Cu. The reason for such behaviour can be attributed to the formation of large amount of intermatallic compounds which are brittle in nature and act as crack propagating sites thus resulting in lower strength and ductility. Fig.5.29 shows the stress vs strain curves for the Al-Cu FSPed samples along with that of pure Al. The UTS and the elongation values for all the 4 samples have been compared in the form of bar diagrams in Fig.5.30.(a) and Fig.5.30.(b) respectively.

Table 10. Measurement of UTS and Maximum Elongation of Al-Cu FSPed samples

S. No.	Compositions	Ultimate Tensile Strength (MPa)	Maximum Elongation (%)
1	Pure Al	153.4	37.8
2	Al-1wt%Cu	187	23.8
3	Al-5wt%Cu	195	15.6
4	Al-10wt%Cu	132.1	5.25

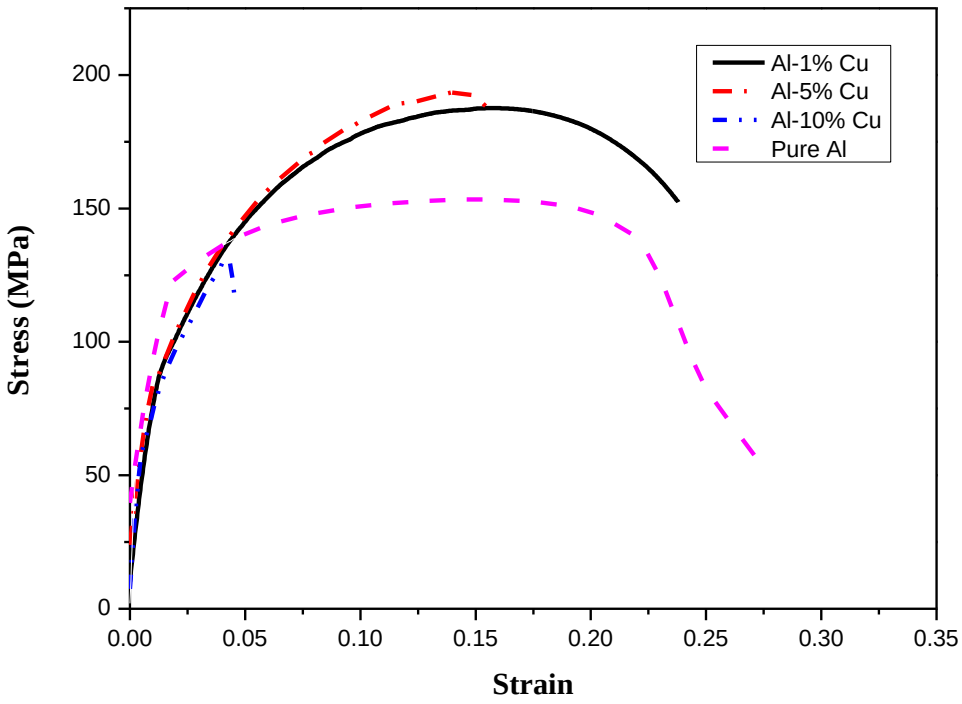

Fig. 5.29. Stress vs strain curves for Al-Cu FSPed samples along with Pure Al

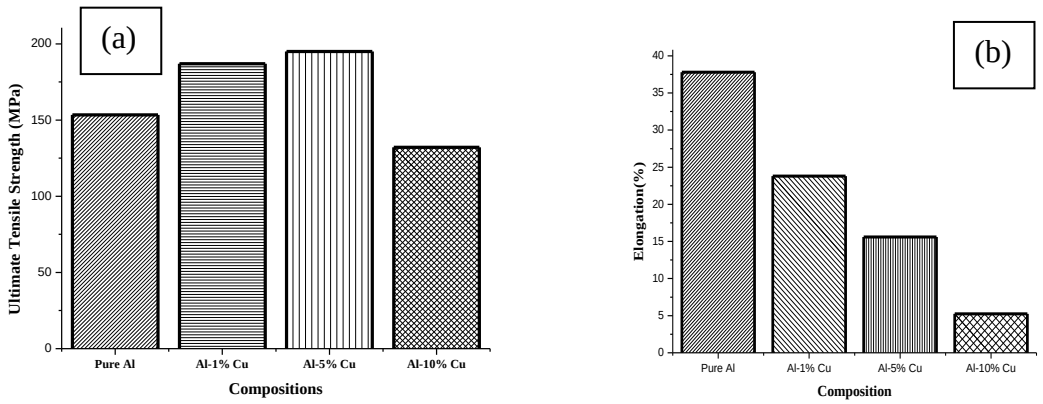

Fig. 5.30. Comparision of (a) UTS and (b) Maximum Elongation values for all 4 samples

5.4.5 Fractrography

Fractured surfaces of the 3 FSPed samples i.e Al-1wt%Cu, Al-5wt%Cu and Al-10wt%Cu were observed under SEM to support the above mechanical properties. The fractographs for Al-1wt%Cu,Al-5wt%Cu and Al-10wt%Cu has been shown in Fig.5.31.(a), Fig.5.31.(b) and Fig.5.31.(c) respectively.In case of Al-10wt%Cu, it was evident from the image of the fractured surface that there was presence of intermetallic compound and crack initiation site was present in it. Due to its presence crack propagated readily resulting in lesser strength and ductility.

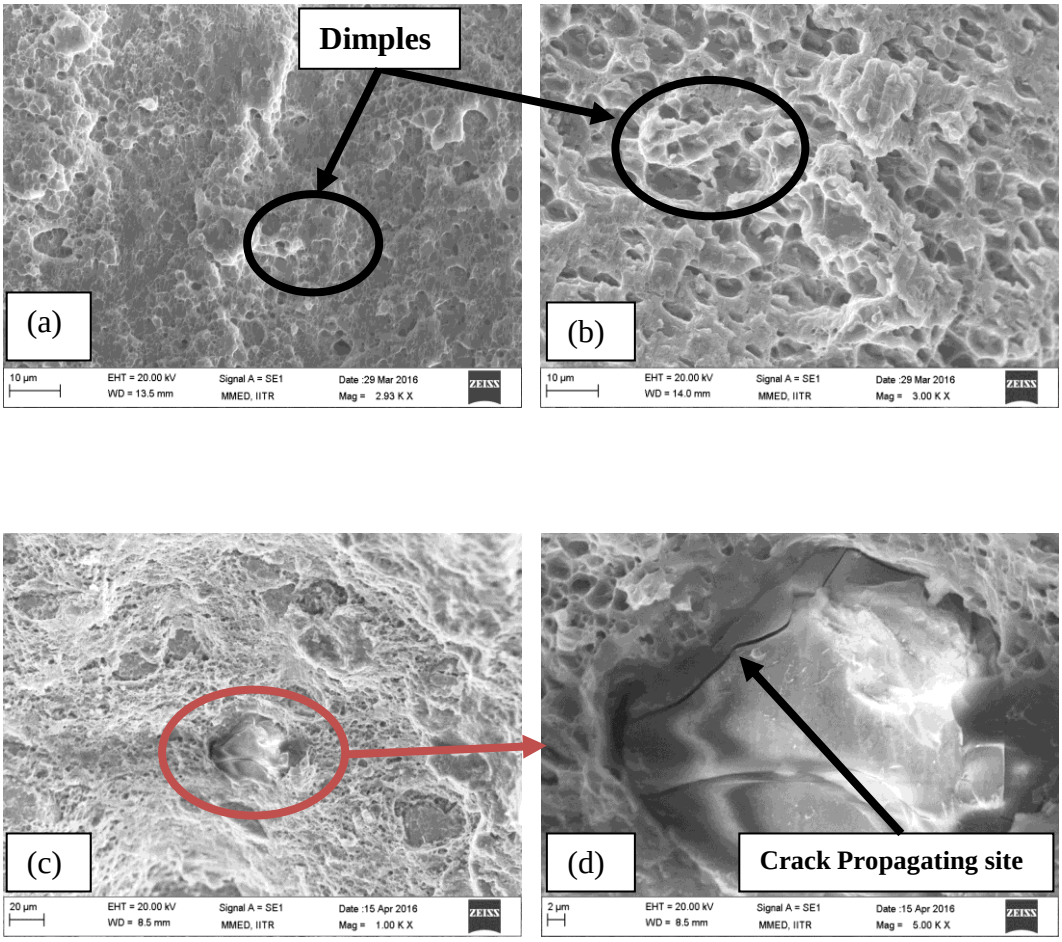

Fig. 5.31. Fractured surface of (a) Al-1wt%Cu FSPed sample and (b) Al-5wt%Cu FSPed sample (c) Fractured surface of Al-10wt%Cu FSPed sample and (d) Region of crack propagation through the intermetallic in case of Al-10%Cu FSPed sample

Chapter 6 CONCLUSIONS

From the above study the following points can be concluded:

(1) Firstly the effect of FSP on the microstructure and mechanical properties of pure Aluminium sample prepared through powder metallurgy route was studied. The main objective was to determine the compaction pressure which is most suitable for performing FSP on the powder sample. So, Cold Isostatic Compaction was done at seven different compaction pressures i.e 50 MPa, 100 MPa, 150 MPa, 200 MPa, 250 MPa, 320 MPa and 380 MPa and subsequently FSP was performed on all the green compacts using process parameters of 1525 rpm rotational speed and 1 mm/min traverse speed. It was found that FSP was possible on all the green compacts and the FSPed sample compacted at 200 MPa showed the best results. This is because at this particular compaction pressure the material movement was occurring as desired and so this particular compaction pressure was selected for further study.

(2) The density values in case of green compacts showed a uniform increase with compaction pressure till 200 MPa compaction pressure after which it showed a decreasing trend mainly due to the spring back effect. In case of FSPed samples there was significant improvement in density and its values almost reached the theoretical density value. The main reason behind this is the complete removal of particle boundaries.

(3) From the EBSD Scan of FSPed region of 200 MPa compacted sample, it was found out that there was significant reduction in grain size after FSP. The average grain size in the stir zone was found to be around 3μm.

(4) The next aim was to compare the green FSPed and sintered FSPed samples compacted at 200 MPa compaction pressure. It was observed that the green FSPed samples showed superior results and so it could be said that the sintering step may be eliminated.

(5) The effect of addition of Cu in Al matrix was desired to be studied. Three Al-Cu mixtures were prepared in which the weight content of Cu was varied i.e Al-1%Cu,Al-5%Cu and Al-10%Cu. They were compacted at 200 MPa and subsequently FSPed using process parameters of 1525 rpm and 1 mm/min. From XRD analysis, it was found that some intermetallic compounds like Al_2Cu etc were formed after FSP which led to enhanced

strength in comparision to pure Al. However in case of Al-10%Cu sample, there was a reduction in strength. This is because of the formation of intermetallics more than desired which acted as crack propagating sites.

(6) Fractography was also carried out in order to support the results. It was found in case of green FSPed sample at 200 MPa there was large amount of dimples of uniform size whereas in case of sintered FSPed sample the dimple size were very uneven. So green FSPed sample showed more ductility. In case of Al-10%Cu sample also the presence of Cu rich intermetallic was clearly seen in the fractured surface and the line of propagation of crack was also visible. Hence it showed very less ductility.

Chapter 7 SCOPE FOR FUTURE WORK

The intermetallic or oxide phases which have formed due to reaction between Al and Cu particles during FSP contribute to strengthening. The strengthening occurring by this mechanism is known as Orowan strengthening. The morphology of these intermetallic compounds may be viewed under TEM in nano scale. Besides copper, other metal powders may also be added to aluminium and similar study may be carried out. In addition to these things as we know that Al-Cu alloy is an age hardenable alloy, so artificial aging may be carried out for different time periods in one of the compositions like: Al-5%Cu. After aging, the precipitates may be viewed under TEM and the improvement in mechanical properties may be studied.

REFERENCES

[1] G. Dowson: Powder Metallurgy- The process and its products, 6th Edition, EPMA, UK, 1992, pp. 1-15

[2] C. Hsu, C. Chang, P. Kao: Al–Al_3Ti nanocomposites produced in situ by friction stir processing, Acta Materialia, 2006, vol 54 (70), pp. 5241- 49.

[3] D. Hull, T. Clyne: An introduction to composite materials, 2nd Edition., Cambridge University Press, Cambridge, 1996, pp. 66

[4] R. Todd, D. Allen, L. Alting: Manufacturing processes reference guide, 1st Edition, Industrial Press Inc., New York, 1994

[5] F. Thummler and W. Thomma: The sintering process, Metallurgical Reviews, No. 115, 1967

[6] R. Mishra, M. Mahoney, S. McFadden, N. Mara, A. Mukherjee: High strain rate superplasticity in a friction stir processed 7075 Al alloy, Scripta Materialia, 2000, vol 42, pp. 163- 68.

[7] R. Mishra, M. Mahoney: Friction stir processing: a new grain refinement technique to achieve high strain rate superplasticity in commercial alloys, Material Science Forum, 2001, vol 357, pp. 507-514.

[8] R. Mishra, Z. Ma: Friction stir welding and processing, Materials Science and Engineering: R: Reports, 2005, vol 50 (1-2), pp. 1-78.

[9] Z. Ma, S. Sharma, R. Mishra: Effect of friction stir processing on the microstructure of cast A356 aluminum, Materials Science and Engineering A, 2006, vol 433; pp. 269– 278.

[10] K.N. Krishnan: On the formation of onion rings in friction stir welds, Materials Science and Engineering,2002, vol A 327, pp. 246-249

[11] A.W. Bowen: Texture development in high strength aluminium alloys, Materials Science Technology,1990, vol 6, pp. 1058-1062

[12] S.Gourder, E.V Konopleva, H.J McQueen, F. Montheillet: Friction stir welding and processing, Material Science Forum, 1996, vol 44, pp. 217-222

[13] K.V Jata, S.L Semiatin: Continuous dynamic recrystallization during friction stir welding of high strength aluminium alloys,Scripta Materialia,2000,vol 43, pp 743-46

[14] J.Q Su, T.W Nelson, R.S Mishra, M.W Mahoney: Microstructural investigation of friction stir welded 7050-T651 aluminium, Acta Materialia, 2003, vol 51, pp. 713-716

[15] Devinder Yadav, Ranjit Bauri: Effect of friction stir processing on microstructure and mechanical properties of aluminium, Materials Science and Engineering, 2012, vol A 539, pp. 85-92

[16] Tjing SC, Ma ZY : Study on mechanical properties of hot extruded Al(Mg)-TiO_2 composites, Materials Science and Engineering, 2000, pp. 29-49

[17] Feng CF, Froyen : In-situ P/M Al/(ZrB_2+Al_2O_3) MMCs: processing, microstructure and mechanical characterization, Acta Materialia, 1999, pp. 47-51

[18] Subramanian R, McKamey CG, Schneibel JH, Buck LR, Menchhofer PA: Microstructure and wear behaviour of Al-Al_2O_3 in situ composites fabricated by the reaction of V_2O_5 on pure aluminium, Materials Science and Engineering, 1998, pp. 254-258

[19] Z. Ma, M. Mahoney, R. Mishra: Superplastic deformation behaviour of friction stir processed 7075Al alloy, Acta Materialia, 2002, vol 50 (17), pp. 4419-4430.

[20] C. Chang, C. Lee, J. Huang: Relationship between grain size and Zener–Holloman parameter during friction stir processing in AZ31 Mg alloys, Scripta Materialia, 2004, vol 51 (6), pp 509-514.

[21] L. Karthikeyan, V. Senthilkumar, V. Balasubramanian, S Natarajan: Mechanical property and microstructural changes during friction stir processing of cast aluminum 2285 alloy, Materials and Design, 2009, vol 30 (6), pp. 2237-2242.

[22] L. Karthikeyan, V. Senthilkumar, K. Padmanabhan: On the role of process variables in the friction stir processing of cast aluminum A319 alloy, Materials and Design, 2010, vol 31 (2), pp. 761-771.

[23] Z.Ma, S. Sharma, R. Mishra: Effect of multiple-pass friction stir processing on microstructure and tensile properties of a cast aluminum–silicon alloy, Scripta Materialia, 2006, vol 54 (9), pp. 1623-1626.

[24] C. Hsu, P. Kao, N. Ho: Ultrafine-grained Al–Al_2Cu composite produced in situ by friction stir processing, Scripta Materialia, 2005, vol 53 (3), pp. 341-345.

[25] Zhang GJ, Bepper Y, Ohji T, Kanzaki S: Effect of tool geometry on shape of nugget zone in friction stir processing, Acta Materialia, 2001, pp. 49-55

[26] I. Lee, P. Kao, N. Ho: Microstructure and mechanical properties of Al–Fe in situ nanocomposite produced by friction stir processing, Intermetallics, 2008, vol 16 (9), pp. 1104-1108.

[27] G. You, N. Ho, P. Kao: In-situ formation of Al_2O_3 nanoparticles during friction stir processing of $AlSiO_2$ composite, Materials Characterization, 2013, vol 80, pp. 1-8.

[28] C. Chen, P. Kao, L. Chang, N. Ho: Effect of processing parameters on microstructure and mechanical properties of an Al-$Al_{11}Ce_3$-Al_2O_3 In-Situ Composite Produced by friction stir processing, Metallurgical and Materials Transactions A, 2009, vol 41 (2), pp. 513-522.

[29] Q. Zhang, B. Xiao, Q. Wang, Z. Ma: In situ Al_3Ti and Al_2O_3 nanoparticles reinforced Al composites produced by friction stir processing in an Al-TiO_2 system, Materials Letters, 2011, vol 65 (13), pp. 2070-2072.

[30] G. You, N. Ho, P. Kao: The microstructure and mechanical properties of an Al–CuO in-situ composite produced using friction stir processing, Materials Letters, 2013, vol 90, pp. 26-29.

[31] G. You, N. Ho, P. Kao: Aluminum based in situ nanocomposite produced from Al–Mg–CuO powder mixture by using friction stir processing, Materials Letters, 2013, vol 100, pp. 219-222.

[32] Z. Liu, B. Xiao, W. Wang, Z. Ma: Singly dispersed carbon nanotube/aluminum composites fabricated by powder metallurgy combined with friction stir processing, Carbon, 2012, vol 50 (5), pp. 1843-1852.

[33] Z. Liu, B. Xiao, W. Wang, Z. Ma: Elevated temperature tensile properties and thermal expansion of CNT/2009Al composites; Composites Science and Technology, 2012, vol 72 (15), pp. 1826-1833.

[34] Y. Kwon, I. Shigematsu, N. Saito: Mechanical properties of fine-grained aluminum alloy produced by friction stir process, Scripta Materialia, 2003, vol 49 (8), pp. 785-789

[35] I.Lee, C. Hsu, C. Chen, N.Ho, P. Kao: Particle-reinforced aluminium matrix composites produced from powder mixtures via friction stir processing, Composites Science and Technology, 2011, vol 71(5), pp. 693-698

[36] H. Izadi, A. Nolting, C. Munro et al.: Friction stir processing of Al/SiC composites fabricated by powder metallurgy, Journal of Materials Processing Technology, 2013, vol 213 (11), pp. 1900-07

LIST OF PUBLICATIONS

Supratim Endow, Aniruddha Malakar, Vivek Pancholi and Vikram V. Dabhade, "**Friction stir processing of sintered powder metallurgical aluminium compacts**", presented at "**International conference on powder metallurgy and particulate materials**", Pune, 18-20 February 2016.